NRC Research Press

ARTICLE

Pargasite-bearing vein in spinel lherzolite from the mantle lithosphere of the North America Cordillera

Edward D. Ghent, Benjamin R. Edwards, and James K. Russell

Abstract: Basanite lavas near Craven Lake, British Columbia, host a spinel lherzolite xenolith containing cross-cutting veins with pargasitic amphibole (plus minor apatite). The occurrence of vein amphibole in spinel lherzolite is singular for the Canadian Cordillera. The vein crosscuts foliated peridotite and is itself cut by the basanite host. The amphibole is pargasite, which is the most common amphibole composition in mantle peridotite. Rare earth element concentrations in the pargasite are similar to those for mafic alkaline rocks across the northern Cordilleran volcanic province (light rare earth elements ~50× chondrite and heavy rare earth elements ~5× chondrite). Two-pyroxene geothermometry suggests that the vein and host peridotite were thermally equilibrated prior to sampling by the basanite magma. Calculated temperature conditions for the sample, assuming equilibration along a model steady-state geotherm, are between 990 and 1050 °C and correspond to a pressure of 0.15 GPa (~52 ± 2 km depth). These conditions are consistent with the stability limits of mantle pargasite in the presence of a fluid having X_{H2O} < ~0.1. The pargasite vein and associated apatite provide direct evidence for postaccretion fracture infiltration of CO_2–F–H_2O-bearing silicate fluids into the Cordilleran mantle lithosphere. Pargasite with low a_{H2O} is in equilibrium with parts per million concentrations of H_2O in mantle olivine, potentially lowering the mechanical strength of the lithospheric mantle underlying the Cordillera and making it more susceptible to processes such as lithospheric delamination. Remelting of Cordilleran mantle lithosphere containing amphibole veins may be involved in the formation of sporadic nephelinite found in the Canadian Cordillera.

Key words: Canadian Cordillera, pargasitic amphibole, mantle xenolith, basanite, apatite.

Résumé : Des laves de basanite près du lac Craven (Colombie-Britannique) renferment un xénolite de lherzolite à spinelle recoupé par des veines contenant de l'amphibole pargasitique (en plus d'apatite en quantité mineure). La présence d'amphibole en veines dans de la lherzolite à spinelle est singulière pour la Cordillère canadienne. La veine recoupe de la péridotite foliée et est elle-même recoupée par la basanite hôte. L'amphibole est de la pargasite, l'amphibole la plus courante dans les péridotites mantelliques. Les concentrations de éléments terres rares dans la pargasite sont semblables à celles de roches alcalines mafiques dans toute la province volcanique du nord de la Cordillère (éléments terres rares légers ~50× chondrite et éléments terres rares lourds ~5× chondrite). La géothermométrie à deux pyroxènes donne à penser que la veine et la péridotite hôte ont subi une équilibration thermique avant l'échantillonnage par le magma basanitique. Les conditions de température calculées pour l'échantillon, en présumant une équilibration le long d'un géotherme modèle stable, sont entre 990 et 1050 °C et correspondent à une pression de 0,15 GPa (profondeur ~52 ± 2 km). Ces conditions concordent avec les limites de stabilité de la pargasite mantellique en présence d'un fluide de X_{H2O} < ~0,1. La veine de pargasite et l'apatite associée fournissent des preuves directes de l'infiltration post-accrétion le long de fractures de fluides silicatés à CO_2–F–H_2O dans la lithosphère mantellique de la Cordillère. De la pargasite de faible a_{H2O} est en équilibre avec des concentrations de H_2O de l'ordre de parties par million dans l'olivine mantellique, réduisant potentiellement la résistance mécanique du manteau lithosphérique qui sous-tend la Cordillère et le rendant plus susceptible à des processus comme la délamination lithosphérique. La refusion de lithosphère mantellique contenant des veines d'amphibole pourrait intervenir dans la formation des néphélinites sporadiquement présentes dans la Cordillère canadienne. [Traduit par la Rédaction]

Mots-clés : Cordillère canadienne, amphibole pargasitique, xénolite mantellique, basinite, apatite.

Introduction

The lithospheric mantle underlying the northwestern Cordillera of North America was formed and modified by a series of complex processes including terrane accretion, subduction, and extension related to postsubduction relaxation and transtension along the Pacific North American plate margin (e.g., Gabrielse and Yorath 1989; Edwards and Russell 1999, 2000; Monger and Price 2002; Francis et al. 2010; Hyndman 2010; Hyndman and Currie 2011; Polat et al. 2018). The resulting lithosphere beneath the British Columbia Cordillera is structurally, compositionally, and mineralogically diverse.

Although geophysical studies have provided broad-scale constraints on the structure and geometry of Cordilleran lithospheric boundaries (e.g., Hyndman and Lewis 1999; Clowes et al. 1995;

Received 15 September 2018. Accepted 7 December 2018.

Paper handled by Associate Editor J. Brendan Murphy.

E.D. Ghent. Department of Earth Science, University of Calgary, Calgary, AB T2N 1N4, Canada.
B.R. Edwards. Department of Earth Sciences, Dickinson College, Carlisle, PA 17013, USA.
J.K. Russell. Department of Earth, Ocean and Atmospheric Sciences, University of British Columbia, Vancouver, BC V6T 1Z4, Canada.
Corresponding author: Benjamin R. Edwards (email: edwardsb@dickinson.edu).

Fig. 1. Geological terrane map of the Canadian Cordillera showing localities of Neogene and Quaternary volcanic centres hosting mantle xenoliths (numbered symbols). Craven Lake volcanic occurrence is indicated by a large symbol (8). Terrane abbreviations are as defined in Colpron and Nelson (2011).

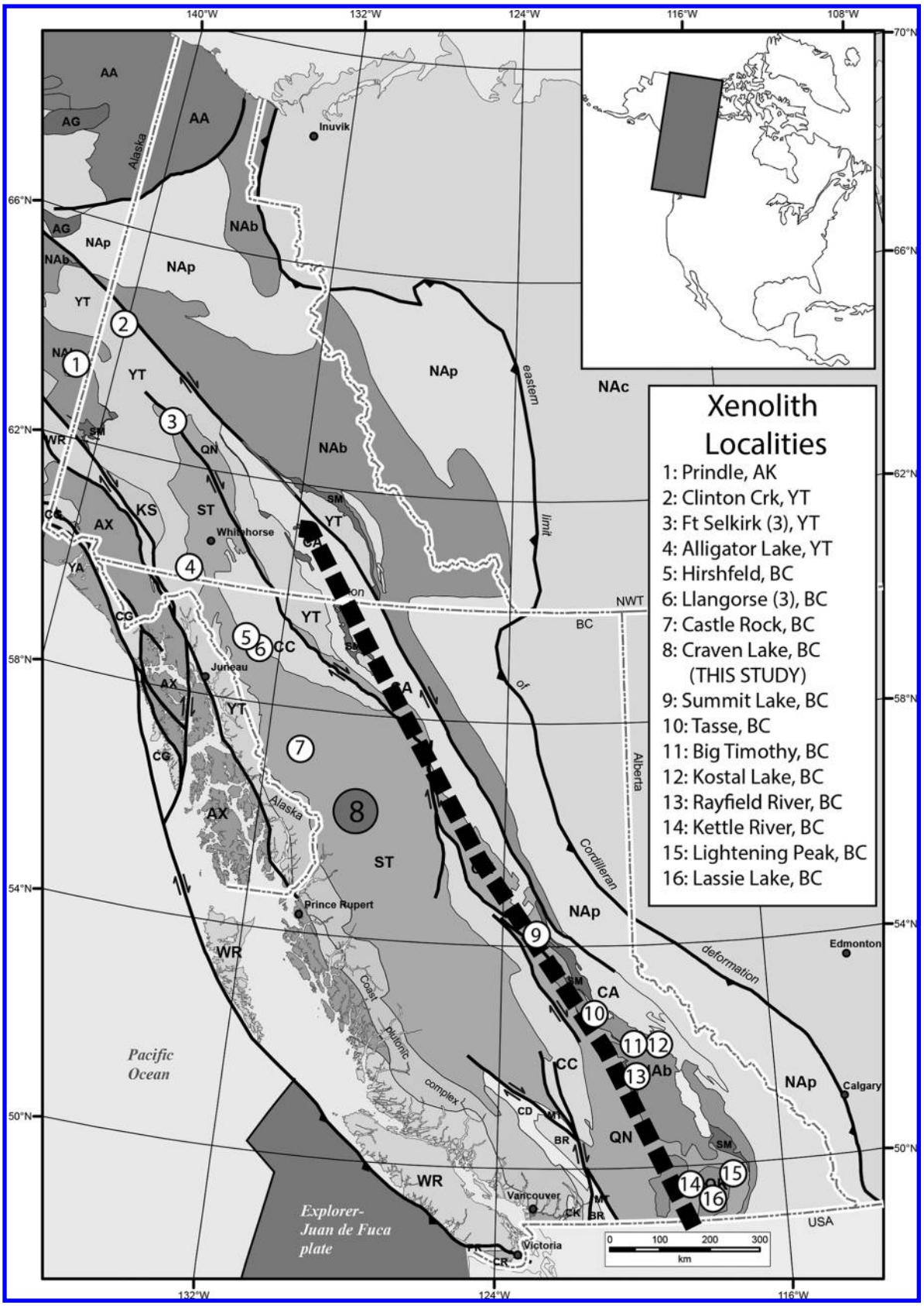

Table 1. Whole-rock chemical compositions of Craven Lake lavas measured by X-ray fluorescence and loss on ignition (LOI) (FeOT calculated from Fe_2O_3 analysis; calculated properties include magnesium number (Mg #) and normative nepheline content (ne)).

	Label			
	04CrL04	04CrL16	04CrL21	04CrL50
Unit	Lower Lp	Lower Lp	Lower Lm	Upper Lp
Latitude	56°54′52″	56°54′56″	56°55′53″	56°54′38″
Longitude	129°21′24″	129°21′58″	129°22′0″	129°23′08″
SiO_2	45.32	45.97	46.21	45.69
TiO_2	2.631	2.526	2.537	2.709
Al_2O_3	14.67	14.80	14.79	14.88
Cr_2O_3	0.021	0.016	0.017	0.022
FeOT	13.42	13.58	13.39	12.97
MnO	0.19	0.19	0.19	0.19
MgO	6.99	6.21	6.61	6.98
CaO	8.26	7.41	7.50	8.39
Na_2O	3.97	4.24	4.58	3.88
K_2O	1.82	2.18	2.16	1.81
P_2O_5	0.815	0.918	0.888	0.831
Total	98.11	98.04	98.87	98.35
LOI	0.76	0.75	0.18	0.59
Mg #	48.2	44.9	46.8	49.0
ne (normative)	9.48	9.52	11.79	8.45

Hammer et al. 2010), much of our knowledge of the lithospheric mantle derives from studies of ultramafic xenoliths transported to the surface by Neogene to Recent volcanism from southeastern British Columbia to easternmost Alaska (Fig. 1) (e.g., Littlejohn and Greenwood 1974; Fiesinger and Nicholls 1977; Brearley et al. 1984; Nicholls et al. 1982; Prescott 1983; Ross 1983; Brearley and Scarfe 1984; Higgins and Allen 1985; Francis 1987; Canil and Scarfe 1989; Canil et al. 1990; Carignan et al. 1994; Shi et al. 1998; Edwards and Russell 2000; Peslier et al. 2000, 2002*a*; Abraham et al. 2005; Harder and Russell 2006; Ghent et al. 2008; Francis et al. 2010; Greenfield et al. 2013; Friedman et al. 2016; Polat et al. 2018). Petrologic and geochemical studies of mantle-derived xenoliths offer a direct means to study the origins, properties, and state of the Cordilleran mantle lithosphere. These studies constrain (*i*) the composition and age of the Cordilleran mantle lithosphere (e.g., Sun and Kerrich 1995; Peslier et al. 2000, 2002*a*, 2002*b*), (*ii*) the structural and geophysical organization of the mantle lithosphere (Littlejohn and Greenwood 1974; Nicholls et al. 1982; Ross 1983; Morales and Tommasi 2011), (*iii*) the presence of hydrous mantle mineral assemblages (Fujii and Scarfe 1982; Brearley et al. 1984; Canil et al. 1987; Canil and Scarfe 1989), (*iv*) the thermal state of the mantle lithosphere (e.g., Ross 1983; Harder and Russell 2006; Currie and Hyndman 2006; Greenfield et al. 2013), (*v*) lithospheric thickness based on xenolith temperatures (e.g., Edwards and Russell 2000; Harder and Russell 2006), and (*vi*) the origins of Neogene to Recent magmatism (e.g., Abraham et al. 2001, 2005; Edwards and Russell 2000; Edwards et al. 2002; Friedman et al. 2016; Polat et al. 2018).

One of the important processes for modifying the chemical composition of the lithospheric mantle over time is the passage of melts and fluids from the asthenosphere into the lithosphere. Episodes of chemical fluxing by fluids from subduction processes or by asthenospheric melts are generally recognized by either "cryptic" changes in compositions of peridotite minerals or the presence of solid phases that require the introduction of fluids to form from peridotite assemblages (O'Reilly and Griffin 2000). These phases include amphibole, mica, apatite, and carbonate minerals (e.g., Francis 1976; Wilshire et al. 1980; Ionov et al. 1996, 1997; O'Reilly and Griffin 2000; Moine et al. 2000). Although volatile-rich minerals can be dispersed as interstitial grains or concentrated in discrete veins, interstitial grains predominate.

Fig. 2. Field photographs of xenoliths in Craven lake volcanic deposits. (A) Outcrop of basanite lava hosting peridotite and pyroxenite xenoliths as well as clinopyroxene megacrysts. (B) Lava sample containing mantle-derived peridotite xenolith juxtaposed with crustally derived gabbro xenolith. (C) Partially fused felsic crustal xenolith in volcaniclastic deposits.

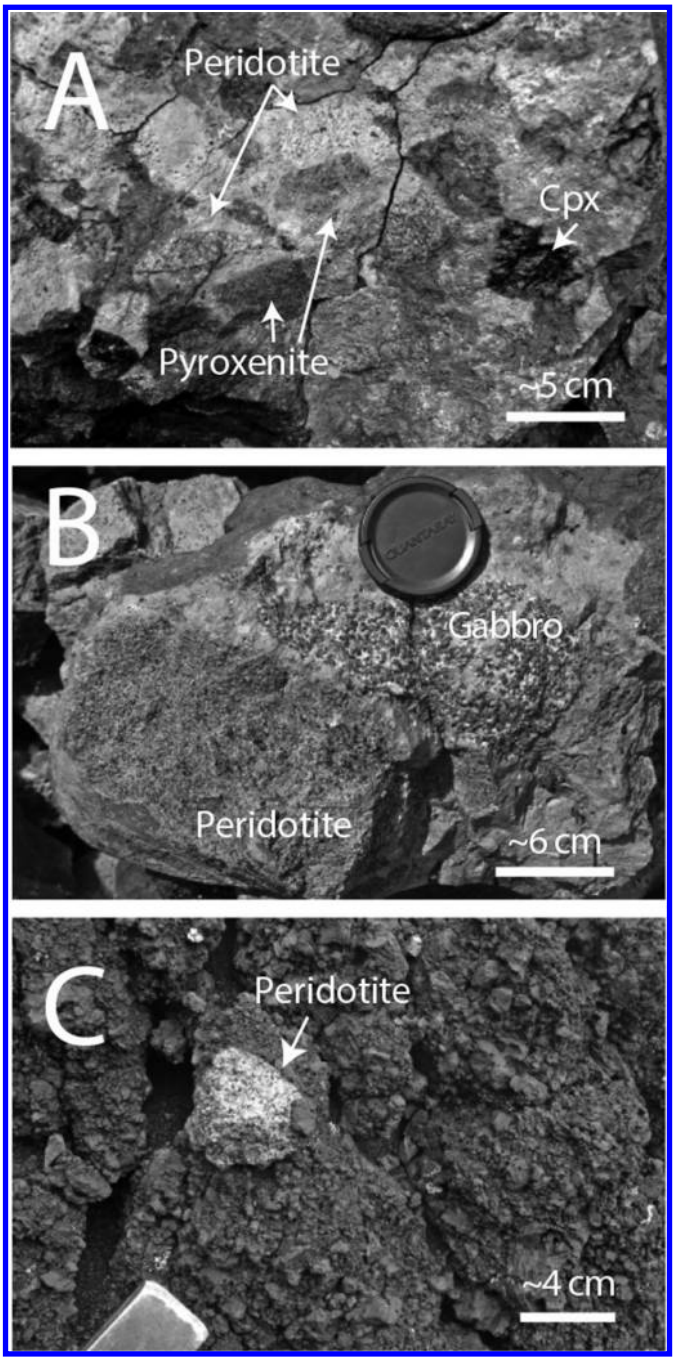

For example, amphibole veins in mantle peridotite xenoliths are relatively uncommon, e.g., spinel harzburgite host in andesite, Avacha volcano, Kamchatka (Ionov 2010; Bénard and Ionov 2013), lherzolite host in basanite, Dish Hill, western United States (Wilshire et al. 1980), lherzolite host in basanite, Spitsbergen, Norway (Ionov et al 1996), and spinel dunite host in basanite, Kerguelen Islands (Moine et al. 2000).

Here we document a new occurrence of an amphibole vein in peridotite collected from basanite tephra near Craven Lake, Brit-

Fig. 3. Photomicrographs of amphibole-bearing lherzolite sample. (A) Digital scan of full-sized thin section (2.5 × 4.25 cm) showing a 2–5 mm wide cross-cutting vein of brown-coloured amphibole. Higher magnification images of amphibole vein (B) where it is fully enclosed by peridotite host and (C) where in contact with basanite lava.

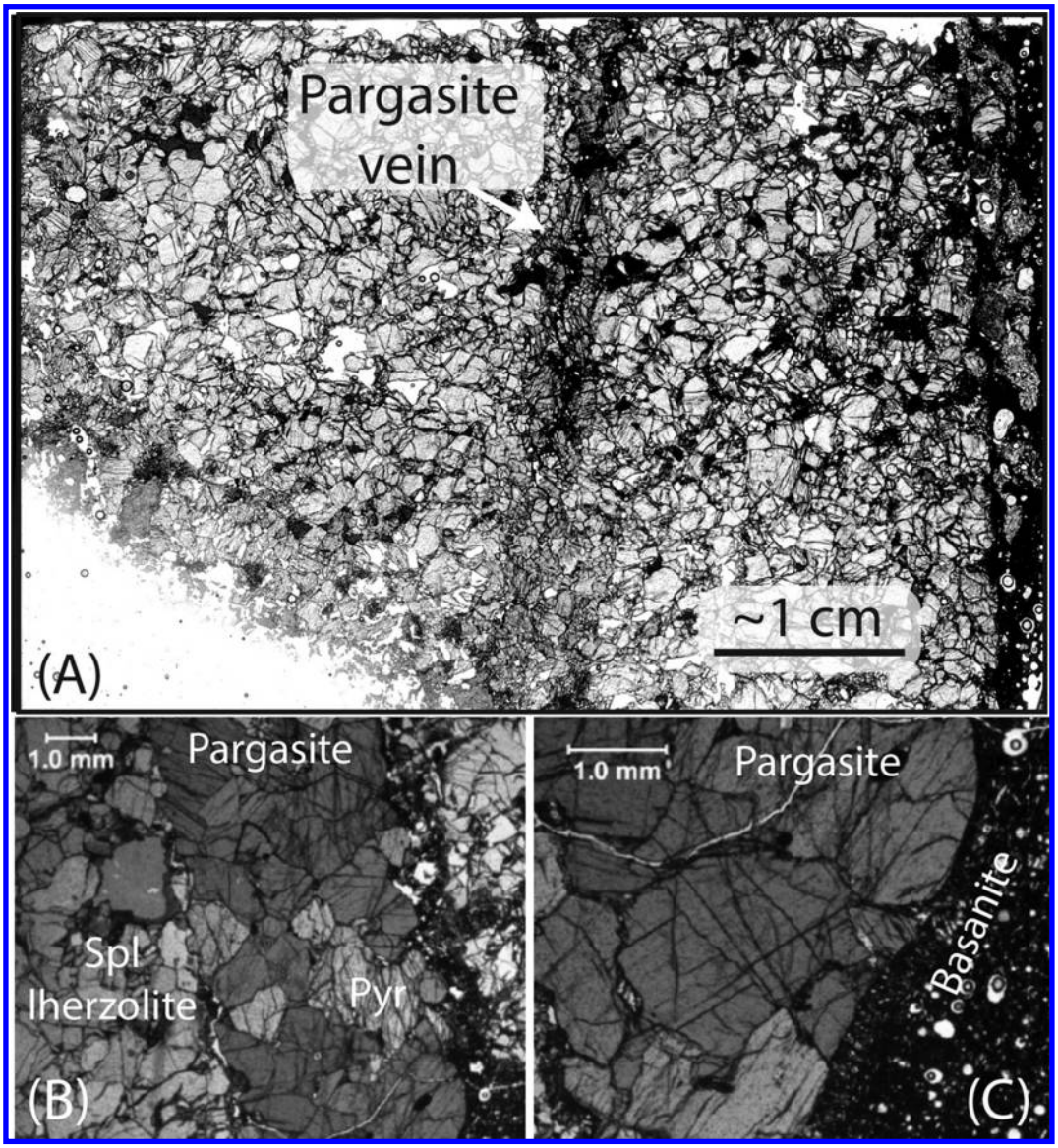

ish Columbia (Fig. 1), which is the first of its kind found in the northern North American Cordillera. We present textural descriptions and new chemical data for the pargasite vein and its host spinel lherzolite xenolith. The pargasite vein (with minor apatite) cross-cuts a poorly developed fabric within the lherzolite. It is also the only reported peridotite xenolith from the northern Cordillera that contains vein-hosted apatite. Both of these phases are important for characterizing the mechanisms of metasomatism affecting the Cordilleran mantle lithosphere and for constraining the nature and origin of the chemical metasomatic agent and its origin (O'Reilly and Griffin 2000). The presence of the vein and its mineral assemblage have significant implications for understanding the rheology of the Cordilleran mantle lithosphere as well as past and future production of mafic alkaline melts.

Geological setting

The Craven Lake volcanic centre is one of 14 mafic volcanic edifices identified within the Bell–Irving volcanic district of the northern Cordillera volcanic province (NCVP) (Edwards and Russell 2000; Edwards et al. 2006). It is situated in the Stikine terrane of the Intermontane Belt within the Canadian Cordillera (Fig. 1). The Bell–Irving volcanic district includes a number of small volcanic centres that erupted through the Bowser Lake Group sediments of the Bowser Basin (Edwards et al. 2006).

The Craven Lake volcanic centre comprises a series of partially dissected pillow mounds situated along a ridgeline to the northwest of Craven Lake and associated mass flow deposits that extend downslope from the pillow-dominated mounds to the valley floor below (~540 m elevation change) (Edwards et al. 2006). The volcanic rocks and deposits are basanite on the basis of whole-rock chemical compositions (Table 1). A sample collected from a neighboring volcanic centre within the Bell–Irving district has an $Ar^{40/39}$ age of 450 ka ± 150 k.y. (Edwards et al. 2006). The similarity in volcanic lithofacies (i.e., pillow lava and palagonitized volcaniclastic deposits) and in degrees of erosion/dissection suggests that the Craven Lake volcanic centre is also Quaternary in age.

Xenoliths occur as lava-coated bombs in volcaniclastic units, within blocks of lava and in pillow lavas. The xenolith suite is

Fig. 4. Element maps for amphibole-bearing vein. (A) Backscattered electron image showing grains of apatite (bright) in amphibole. X-ray element maps of (B) Al map with brightest Al in Cr-spinel, (C) Ca map with brightest Ca in apatite, (D) Fe map with brightest Fe in iron oxides, (E) K map with bright K in pargasite;,and (F) Ti map with brightest Ti showing pargasite intergrown with orthopyroxene. All images are at the same scale.

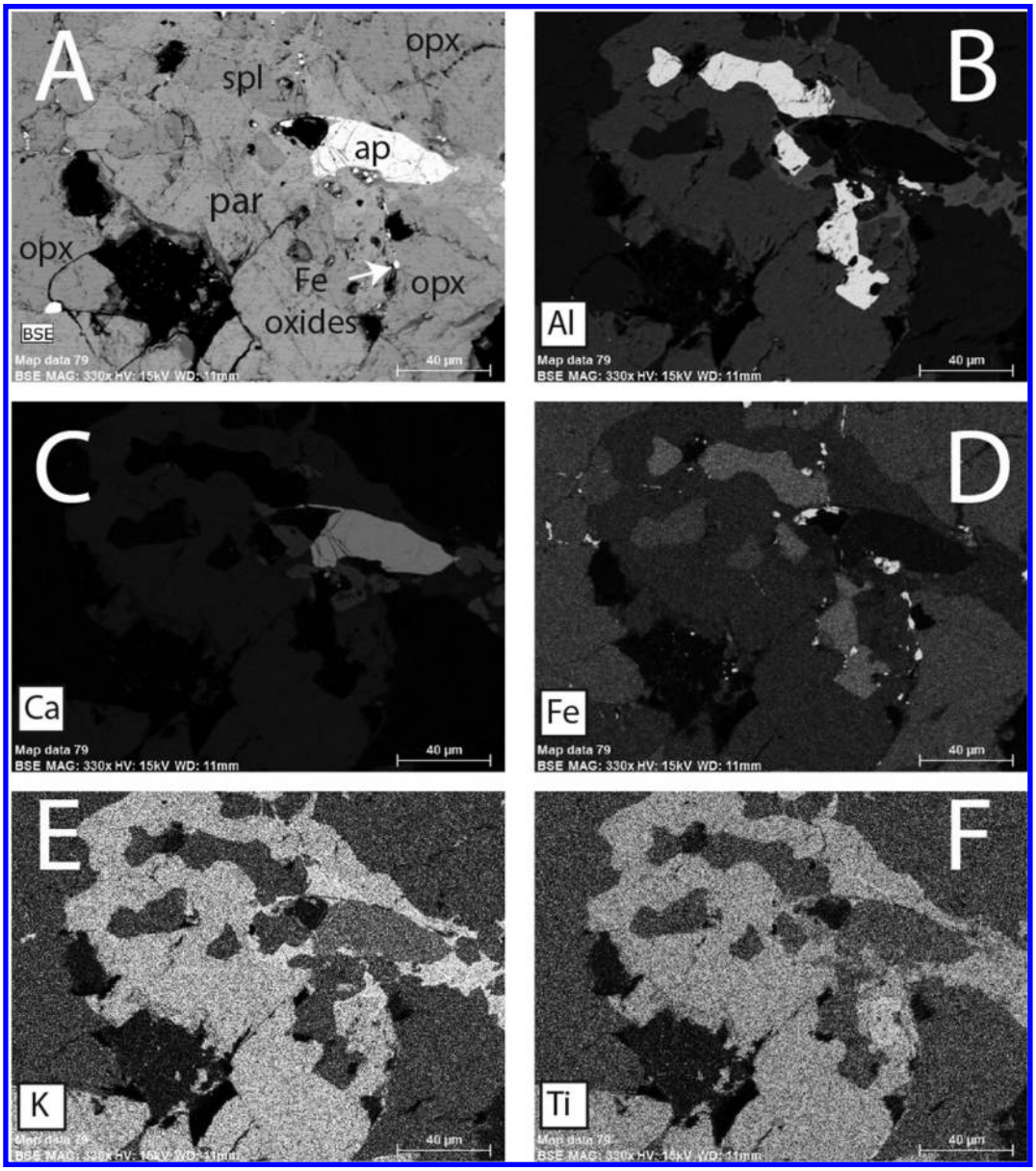

relatively diverse, including a variety of peridotites, crustally derived rocks and large megacrysts of clinopyroxene and plagioclase (Fig. 2) (Miller et al. 2010). Approximately 60 xenoliths were collected and examined. A single sample of spinel lherzolite was found that contains a vein of amphibole (VT09/09CM10) (Fig. 3).

Xenolith textures

The peridotite xenolith containing the amphibole vein is a spinel lherzolite and has a primary mineralogy of olivine, orthopyroxene, clinopyroxene, and spinel. The spinel lherzolite has a protoclastic texture (Fig. 3) comprising extremely irregular grain shapes and an average grain size of ~1.0 to 1.50 mm. Deformation bands in olivine and subgrain formation at grain edges are common. The lherzolite is cut by a ~3 mm wide vein of brown-pleochroic amphibole (Fig. 3). Apatite grains occur adjacent to the vein and within the lherzolite matrix at several millimetres from the amphibole vein. A thin "microveinlet" with complex mineralogy and textures is in contact with the amphibole vein and is described in more detail below. The principal vein locally has sharp contacts with the host spinel lherzolite. The brown amphibole grains have irregular shapes and are ≤1 mm in maximum dimension but typically much finer grained (Fig. 3).

Apatite is typically associated with vein amphibole and occurs as elongate anhedral crystals (Fig. 4A). Anhedral crystals of spinel (high Al) are found in contact with amphibole (lower Al) (Fig. 4B). Apatite (Fig. 4C) (high Ca) and granular iron oxides (Fig. 4D) (high-Fe) are also in contact with amphibole. Amphibole (Fig. 4E) (high K) occurs with inclusions of orthopyroxene (Fig. 4F) (low Ti).

Mineral compositions

Major and minor elements

Major and minor element concentrations in mantle phases were analyzed using a JEOL 8200 electron probe microanalyzer at

Table 2. Compositions (weight percent, measured by an electron probe microanalyzer) and cation abundances (AX program) of coexisting orthopyroxene and clinopyroxene used for geothermometry.

Oxide	opx-K101	cpx-K101	opx-K102	cpx-K102	opx-K103	px-K103
SiO_2	54.66	52.19	55.15	52.04	54.1	52.23
TiO_2	0.10	0.45	0.13	0.47	0.11	0.41
Al_2O_3	4.95	6.60	4.96	6.80	4.68	7.00
Fe_2O_3	1.49	1.16	0.71	1.04	1.24	1.24
FeO	6.76	2.53	6.43	2.14	9.42	3.79
MnO	0.12	0.10	0.17	0.07	0.21	0.14
MgO	32.04	15.28	32.55	15.34	29.90	14.70
CaO	0.09	20.25	0.81	20.51	0.88	19.36
Na_2O		1.51	0.09	1.47	0.16	1.70
Sum	100.21	100.07	101.00	99.88	100.70	100.57
Cations on the basis of 6 oxygens and 4 cations						
Si	1.881	1.878	1.890	1.880	1.890	1.883
Ti	0.003	0.012	0.003	0.013	0.003	0.011
Al	0.201	0.293	0.200	0.290	0.193	0.298
Fe^{3+}	0.038	0.031	0.018	0.028	0.033	0.033
Fe^{2+}	0.195	0.076	0.184	0.065	0.275	0.114
Mn	0.003	0.003	0.005	0.002	0.006	0.004
Mg	1.643	0.82	1.663	0.826	1.557	0.790
Ca	0.006	0.781	0.03	0.794	0.033	0.748
Na		0.105	0.006	0.103	0.011	0.119

Table 3. Compositions (weigh percent, measured by an electron probe microanalyzer) and cation abundances of olivine adjacent to the vein and within the matrix.

Oxide	Olivine #7	Olivine #11	Olivine core	Olivine trav.	Olivine rim
SiO_2	40.50	39.39	39.54	39.81	40.19
FeO	11.43	12.50	15.75	15.63	13.08
MnO	0.13	0.16	0.20	0.16	0.14
CaO	0.33	0.37	0.34	0.38	0.34
NiO	0.33	0.07	0.08	0.08	0.16
MgO	0.06	47.38	44.13	44.45	45.83
Sum	99.72	99.87	100.04	100.51	99.74
Cations on the basis of 4 oxygens and 3 cations					
Si	1.00	0.98	1.00	1.00	1.00
Fe	0.24	0.26	0.33	0.33	0.27
Mn	0.003	0.003	0.004	0.003	0.003
NiO	0.007	0.003	0.007	0.008	0.007
Ca	0.002	0.002	0.002	0.002	0.004
Mg	1.75	1.76	1.66	1.66	1.71
Sum	3.002	3.008	3.003	3.003	2.994
Mol % Fo	88	88	83	83	86

Note: Olivine #7 and #11 are from the xenolith matrix away from vein; olivine core, trav., and rim are olivine near the vein and an analytical traverse from core to rim. *Mol % Fo is the molecular percentage of the forsterite endmember calculated as Mg cations/(Mg cations + Fe cations).

the Department of Geoscience, University of Calgary. Operating conditions for the electron microprobe were accelerating voltage 15 kV, beam current 100 nA, and beam diameter about 5 μm (cf. Greenfield et al. 2013). We report representative compositions of pairs of orthopyroxene and clinopyroxene grains used in geothermometry (Table 2), major and minor element compositions of olivine (Table 3) and spinel (Table 4), and major and trace element compositions of amphibole (Tables 5 and 6; Fig. 5) and apatite (Table 7). The number of atoms per formula unit for all minerals except apatite have been calculated in the program AX written by Tim Holland (available on his software page, also see Holland and Powell 1998).

Compositions of orthopyroxene, clinopyroxene, and olivine crystals away from the vein are similar to those from other suites of mantle xenoliths reported from the Canadian Cordillera (e.g., Greenfield et al. 2013; Table 2). Olivine crystals adjacent to the vein are reversely zoned ($Fo_{83–86}$) and have lower Fo contents than those in away from the vein (Fo_{88}) (Table 3).

Representative analyses of spinel (Table 4) were normalized to three cations to estimate the amount of ferric iron. Spinel has variable composition; $Fe^{3+}/[Fe^{3+} + Fe^{2+}]$ atomic ratios range from 0.19 to 0.24. The Cr_2O_3 contents of spinel in the matrix are high, ranging from 9.5 to 10.4 wt.%.

We have classified the vein amphibole compositions by calculating apfu of Al + Fe^{3+} + 2Ti versus Na + K + 2Ca on a diagram A = (Na + K +2 Ca) and C = (Al + Fe^{3+} +2Ti) following the recommendation of Hawthorne et al. (2012) (Fig. 5A). All of the new amphibole analyses plot in the pargasite field, which is the most common amphibole found in upper mantle peridotitic xenoliths (Dawson and Smith 1982). To facilitate comparison of the compositions of our vein amphibole (Table 5) to published analyses from other peridotitic occurrences of amphibole, we have recalculated all amphibole compositions to cations on the basis of the formula, $AX_2Z_5(Si, Al, Ti)_8O_{22}(OH, F, Cl, O)_2$ (Hawthorne et al. 2012; Holland and Powell 1998). The same recalculated formulas with activities of the components were used in the phase equilibria described

Table 4. Compositions (weight percent, measured by an electron probe microanalyzer) of spinel within peridotite xenolith.

Oxide	7	10	12	14	15	16	17	18
SiO_2	0.00	0.00	0.00	0.00	0.00	0.00	0.00	0.00
TiO_2	0.12	0.10	0.12	0.11	0.10	0.10	0.56	0.61
Cr_2O_3	10.44	9.58	9.47	8.23	8.26	8.23	15.67	17.13
Al_2O_3	51.67	54.3	54.08	57.37	57.57	57.37	49.80	48.17
$Fe_2O_3^{\dagger}$	5.51	4.02	4.36	1.94	2.00	2.35	2.85	2.63
FeO	15.47	15.4	14.93	13.73	13.65	15.44	11.42	11.65
MnO	0.16	0.18	0.13	0.10	0.10	0.14	0.14	0.16
NiO	0.29	0.34	0.32	nd	nd	nd	nd	nd
MgO	15.61	16.26	16.4	17.70	17.85	18.03	18.49	18.17
Sum	99.27	100.18	99.81	99.18	99.55	99.54	99.23	98.62
Number of cations normalized to 3								
Ti	0.002	0.002	0.002	0.002	0.002	0.002	0.011	0.013
Cr	0.225	0.202	0.204	0.172	0.172	0.171	0.334	0.370
Al	1.661	1.711	1.707	1.785	1.784	1.778	1.585	1.551
Fe^{3+}	0.113	0.081	0.088	0.039	0.040	0.046	0.058	0.054
Fe^{2+}	0.352	0.345	0.335	0.303	3.000	0.293	0.258	0.266
Mn	0.003	0.004	0.003	0.002	0.002	0.003	0.010	0.004
Ni	0.007	0.007	0.007	nd	nd	nd	nd	nd
Mg	0.634	0.647	0.655	0.697	0.700	0.706	0.742	0.740

Note: Analyses 17 and 18 are from spinel hosted in "veinlet" (see text).
*Ferric iron estimated by normalizing cations to 3 using program AX.
nd denotes elements not analyzed for SiO_2 was below detection limits.

Table 5. Compositions (weight percent, measured by an electron probe microanalyzer) of pargasite within veins hosted by peridotite xenolith.

	3	4	5	6	7	8	17	18	19
SiO_2	43.28	42.99	43.07	43.25	43.10	43.34	43.43	43.29	42.94
TiO_2	2.06	2.06	2.13	2.06	2.12	2.08	2.11	2.06	2.10
Al_2O_3	16.48	16.36	16.43	16.37	16.3	16.36	16.42	16.53	16.55
Cr_2O_3	0.25	0.29	0.25	0.22	0.26	0.23	0.14	0.16	0.10
Fe_2O_3	2.37	2.43	2.42	2.42	2.31	2.36	2.40	2.40	2.43
FeO	2.15	2.21	2.20	2.20	2.10	2.15	2.19	2.19	2.21
MnO	0.08	0.08	0.04	0.08	0.06	0.03	0.07	0.06	0.06
MgO	17.36	17.19	17.36	17.28	17.38	17.48	17.33	17.21	17.25
CaO	11.06	11.06	10.98	11.11	11.09	10.98	11.05	11.15	11.10
Na_2O	3.06	3.02	2.99	2.96	3.09	3.03	3.01	3.05	3.03
K_2O	1.22	1.24	1.24	1.26	1.21	1.24	1.21	1.22	1.21
Sum	99.13	98.68	98.87	98.97	98.79	99.04	99.12	99.08	98.73
Number of atoms on the basis of 23 oxygens									
Si	6.029	6.022	6.017	6.037	6.026	6.040	6.047	6.033	6.008
Ti	0.216	0.217	0.224	0.216	0.223	0.218	0.221	0.216	0.221
Al	2.707	2.702	2.706	2.694	2.687	2.688	2.695	2.716	2.730
Cr	0.028	0.032	0.028	0.024	0.029	0.025	0.015	0.018	0.011
Fe^{3+}	0.248	0.256	0.254	0.254	0.243	0.247	0.252	0.252	0.255
Fe^{2+}	0.251	0.259	0.257	0.257	0.246	0.250	0.255	0.255	0.258
Mn	0.009	0.009	0.005	0.009	0.007	0.004	0.008	0.007	0.007
Mg	3.604	3.589	3.615	3.595	3.622	3.630	3.596	3.575	3.597
Ca	1.651	1.66	1.644	1.662	1.662	1.640	1.648	1.665	1.664
Na	0.827	0.82	0.81	0.801	0.838	0.819	0.813	0.824	0.822
K	0.217	0.222	0.221	0.224	0.216	0.220	0.215	0.217	0.216
Sum	15.87	15.88	15.87	15.86	15.88	15.87	15.85	15.86	15.88

Note: Ferric iron after Holland and Blundy (1994). Mixing on sites from Holland and Powell (1998).

below. We have compiled amphibole compositions from four other mantle peridotite occurrences (Frey and Green 1974; Francis 1976; Brearley and Scarfe 1984; Dawson and Smith 1982) including three from western North America. We also plotted compositions of amphiboles produced in high-temperature–pressure experiments simulating metasomatism of lherzolite (Sen and Dunn 1995) and edenitic amphiboles found within peridotitic xenoliths within andesite from Avacha volcano, Kamchatka (Bénard and Ionov 2013).

As expected, based on the review of Dawson and Smith (1982), our amphiboles are pargasite as are all other mantle-peridotite-hosted amphiboles (Fig. 5A). The sole exception is the amphibole recovered from mantle xenoliths hosted in andesite (Bénard and Ionov 2013). Earlier work of Wilshire et al. (1980) showed that the most common amphibole found in pyroxene-bearing veins within Cr-diopside xenoliths was kaersutite. Wilshire et al. (1980) noted that the amphibole compositions varied between kaersutite within veins to more pargasitic compositions in the matrix of the host peridotite. Recalculation of Wilshire's average analyses yields $(Al + Fe^{3+} + 2Ti) = 1.318$ and $^{A}(Na + K + 2Ca) = 0.746$ in vein amphiboles and $(Al + Fe^{3+} + 2Ti) = 1.297$ and $^{A}(Na + K + 2Ca) = 0.581$ in matrix amphiboles. These also plot in the pargasite field.

Table 6. Trace and minor element compositions (ppm) of pargasite in veins (averages of 20 spots per vein).

	Vein 1		Vein 2		Detection limit (2 sigma)
Ti	11607	±839	10537	±804	100
Rb	697	±0.8	654	±0.8	7
Sr	971	±80	982	±157	8
Y	21.85	±0.5	20.3	±0.5	1
Zr	289	±35	265	±38	3
Nb	58.1	±6.9	50.6	±5.9	0.8
La	13	±0.6	12.8	±0.6	0.3
Ce	37.9	±1.9	36.3	±1.7	0.5
Pr	5.99	±0.34	5.53	±0.30	0.16
Nd	32.7	±2.5	29.9	±1.7	0.8
Sm	9.06	±0.8	8.06	±0.5	0.5
Eu	3.04	±0.2	2.83	±0.15	0.15
Gd	8.61	±0.85	7.52	±0.49	0.45
Tb	1.19	±0.09	0.98	±0.06	0.06
Dy	5.42	±0.25	4.91	±0.34	0.28
Ho	0.85	±0.05	0.81	±0.06	0.06
Er	1.88	±0.13	1.8	±0.11	0.12
Tm	0.22	±0.02	0.22	±0.02	0.03
Yb	1.33	±0.14	1.31	±0.11	0.15
Lu	0.17	±0.03	0.18	±0.01	0.03
Ta	4.18	±0.78	3.67	±0.66	0.14

Apatite crystals occur associated with the pargasite vein and less commonly within the peridotite matrix. Crystals are irregular to blocky shapes with sizes ranging from about 20 to 40 μm. Electron microprobe analyses were recalculated using the normalization routine in an apatite stoichiometry program (Ketcham 2015). The recalculated formulas indicate that the apatites are rich in F and Cl with little or no OH^- (Table 7).

Trace element analyses and interpretation for vein amphibole

Trace element compositions of amphiboles were measured at the University of Calgary, Center for Pure and Applied Tectonics and Thermochronology (CPATT), using a laser ablation inductively coupled plasma mass spectrometer (LA-ICP-MS) (Table 6). Isotope signal intensities were measured using an Agilent 7700 quadrupole ICP-MS coupled to a Resonetics RESOchron 193 nm excimer laser ablation system. Ablation was conducted in a Laurin Technic M-50 dual volume ablation cell. Laser settings, dwell times for individual masses, gas flow rates, and mass spectrometer settings can be found in the supplementary information;[1] more information about the laser ablation system used can be found in Müller et al. (2009). The well-characterized NIST610 glass was used as a calibration reference material (Pearce et al. 1997; Jochum et al. 2011). A sample-standard bracketing approach was used with one measurement of the calibration reference between each two unknowns. Data was reduced using the commercially available Iolite software (V2.5) package (Paton et al. 2010) using the TraceElements data reduction scheme.

We have compared the chondrite-normalized (Boynton 1984) rare earth element compositions of Craven Lake amphibole (Table 6) to other "local" mantle geochemical reservoirs, including peridotite mantle from the North American cratonic mantle and the Cordilleran mantle and Quaternary alkali olivine basalt and nephelinite from the Canadian Cordillera (Figs. 5B and 5C). Our amphiboles are enriched relative to both types of depleted peridotites, showing light rare earth element patterns that are in between asthenospheric (alkali olivine basalt) and lithosphere (nephelinite) melts; middle rare earth element and heavy rare earth element values are more similar to nephelinite magmas than alkali olivine basalts.

The Craven Lake mantle amphiboles are also compared to Group 1 and 2 mantle-hosted amphiboles after Bénard and Ionov (2013) (Fig. 5C). Group 1 are thought to derive from mantle-derived melts-fluids forming by interactions below the Moho. Group 2 are interpreted to result from interactions with host andesites above the Moho (i.e., amphibole in Avancha peridotite xenoliths from a andesite host). The Craven Lake occurrence has higher light rare earth element abundances that do not match either data set (i.e., Group 1 or 2).

Geothermometry results

Temperatures for the spinel lherzolite were estimated using the Brey and Kőhler (BK) (1990) orthopyroxene–clinopyroxene geothermometer. The coexisting pyroxenes were analyzed where they were in contact. The BK geothermometer has a slight pressure dependence (~2 °C·kbar^{-1}) and to account for this, we assume the mantle xenolith record temperatures along the mantle geotherm following the work of Kukkonen and Peltonen (1999), Harder and Russell (2006) and Greenfield et al. (2013). We achieve a pressure-dependent estimate of mantle temperature by solving the BK equation simultaneously with the expected steady-state temperature distribution in the mantle lithosphere described by

$$T(z) = T_M + (z - z_M)(q_0 - 0.63212A_0z_M/K) \quad (1)$$

where K is the thermal conductivity of the mantle lithosphere and T_M and z_M are the temperature and depth of the Moho, respectively (e.g., Greenfield et al. 2013). The mantle temperature–depth array also depends on the properties of the overlying crustal layer including surface heat flow (q_0) and crustal heat production (A_0). Lithoprobe seismic reflection surveys over northern British Columbia have shown the Moho to be located at depths of ~36 ± 2 km (Hammer et al. 2000; Hammer and Clowes 2004; Clowes et al. 2011). Here we adopt a model MOHO depth (Z_M) of 36 km. We also assume a Moho temperature of 825 ± 25 °C based on the work of Harder and Russell (2006) and Greenfield et al. (2013) and, recently, adopted by Hyndman (2017; 800–850 °C; see references therein). Estimates for surface heat flow (q_0; 47 and 55 mW·m^{-2}) and crustal heat production (A_0; 1.75 μW·m^{-3}) for this portion of the Cordillera are taken from Lewis et al. (1992) (cf. Hyndman 2010).

The BK equation has two unknowns, including the temperature and the pressure of equilibration, and the equation for the mantle geotherm is dependent only on depth (i.e., z). We can rewrite the variable z in eq. 1 in terms of pressure and solve the BK equation and eq. 1 simultaneously for temperature and pressure (Table 8; Fig. 6) (after Greenfield et al. 2013). The model P–T values have the attribute of being consistent with the compositions of coexisting pyroxenes and lying on the local model geotherm (Fig. 6).

Temperatures and pressures were calculated with this strategy for the host spinel lherzolite (i.e., matrix) and for pyroxene pairs within or adjacent to the amphibole-bearing vein (Table 8). Six pairs of pyroxenes from the host peridotite record a mean temperature of 1012 ± 21 °C whilst four pairs adjacent to the vein amphibole are slightly higher 1032 ± 20 °C but are within the uncertainties of the method (Fig. 6).

Constraints on volatile components

One of the most significant aspects of finding volatile-bearing minerals from the lithospheric mantle is that the minerals can provide constraints on the activities of components in the fluid

[1]Supplementary data are available with the article through the journal Web site at http://nrcresearchpress.com/doi/suppl/10.1139/cjes-2018-0239.

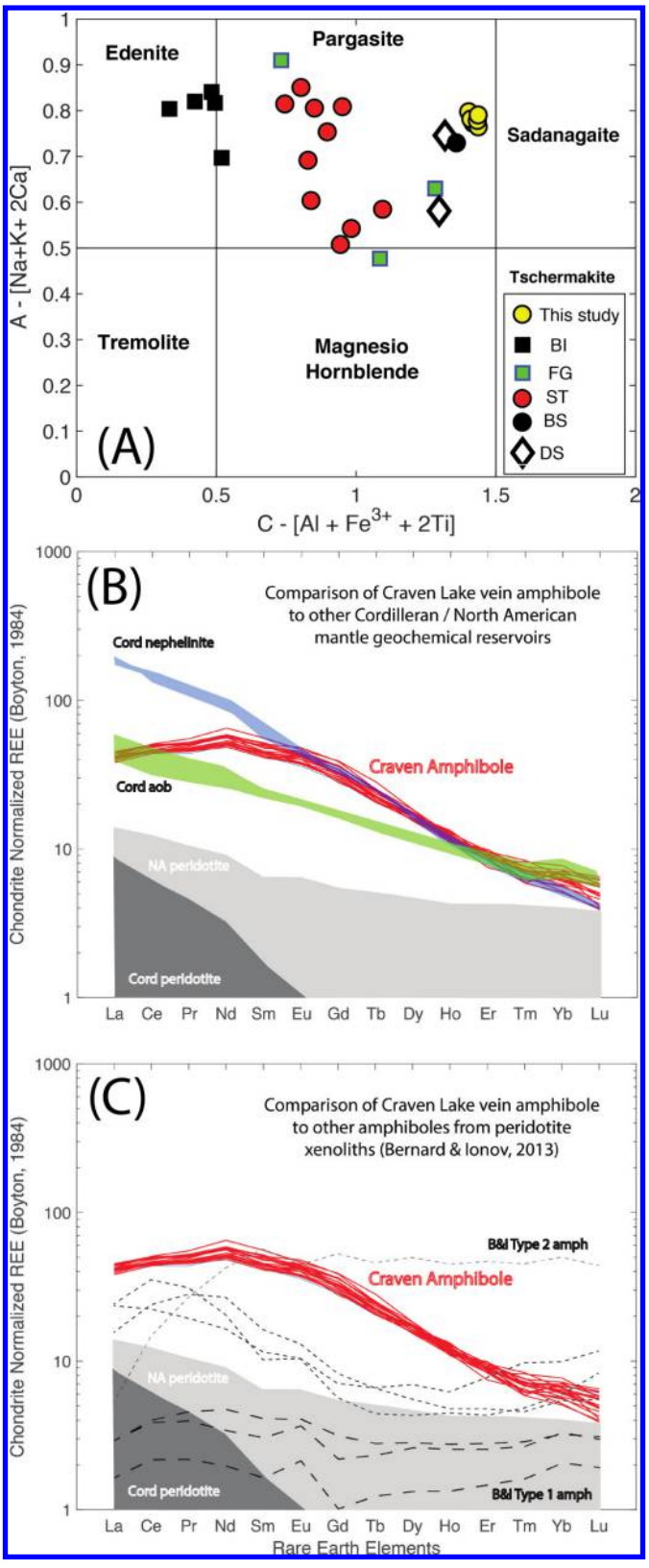

Fig. 5. Compositions of amphibole. (A) Compositions of amphibole (Table 5) plotted as apfu of (Al + Fe^{3+} + 2Ti) versus (^{A}Na + K + 2Ca) on a classification diagram (Hawthorne et al. 2012). Vein amphibole in the Carven lake peridotite sample is pargasitic as are amphiboles reported from other mantle peridotites: DS (Dawson and Smith 1982), BS (Brearley and Scarfe 1984), and FG (Frey and Green 1974). Also shown are amphiboles produced in high-temperature–pressure experiments simulating metasomatism of lherzolite: ST (Sen and Dunn 1995) and edenitic amphiboles within peridotitic xenoliths from Avacha volcano, Kamchatka (BI): (Bénard and Ionov 2013). (B) Rare earth element (REE) compositions of Craven Lake amphibole (Table 6) normalized to chondrite abundances (Boynton 1984) and compared to REE data for peridotite North American and Cordilleran mantle and alkaline basalts and nephelenites from the Canadian Cordillera. (C) The same data compared to Group 1 and 2 mantle-hosted amphiboles after Bénard and Ionov (2013).

phases that were present when the minerals formed (e.g., Lamb and Popp 2009). This information can be useful for assessing (*i*) the impact of tectonic processes on the formation of the lithosphere, (*ii*) the potential for hydration of mantle olivine to change the rheology of the northern Cordillera mantle lithosphere (e.g., Dixon et al. 2004), and (*iii*) the production of lithospheric melts during periods of transtension or increased asthenospheric heat flow (e.g., Francis and Ludden 1990). Below we have used the pargasite presence in the veins to calculate the activities of volatile species (H_2O and CO_2) and their implications for mantle lithospheric processes. The higher Fe content of olivine near the pargasite vein is likely due to reactions between the vein-producing fluids and preexiting olivine with lower Fe content. The presence of relatively high F/Cl and low H_2O in apatite is also significant for constraining the origin of the fluid phase.

Constraints from pargasite

We have investigated the stability of Ca-amphibole using similar principles but different equilibria from those used by Lamb and Popp (2009). Our chosen equilibria involve the activities of pargasite and a mantle mineral assemblage (clinopyroxene, orthopyroxene, and olivine). We have estimated the activity of SiO_2 in the absence of a SiO_2 polymorph (i.e., quartz) using the equilibrium

(2) Forsterite + SiO_2 = Enstatite

The calculations made use of the THERMOCALC program in Holland and Powell (1998). The *P*–*T*–a_{H2O} values used in the calculations below and in Fig. 7 are based on the geotherm-constrained temperatures calculated from the orthopyroxene–clinopyroxene geothermometer (*T* ~900–1100 at *P* ~15 kbar (1 kbar = 0.1 GPa)) (Fig. 6; Table 8). At 1000 °C and 15 kbar, the activities of forsterite and enstatite are 0.55 and 0.68, respectively. The implied equilibrium value for a_{SiO2} from eq. 2 is ~0.5.

To compute the stability of pargasite under mantle *P*–*T*–fluid conditions, we estimated the relevant activities of components in the mantle mineral solid solutions using the program AX in HERMOCALC 2007 (Holland and Powell 1998) for a range of mantle conditions (i.e.,*T*–*P*). The activity values that we adopted include pargasite (0.21), forsterite (0.55), enstatite (0.68), diopside (0.60), Mg-Tschermak (0.07), jadeite (0.10), and SiO_2 (0.5).

We consider two equilibria (Fig. 7A) that use mantle mineralogy to constrain the a_{H2O}. The equilibrium

(3) 2 pargasite + 3 SiO_2 = forsterite + 2 jadeite + 4 diopside + 2 Mg-Tschermak + 2 H_2O

constrains a_{H2O} at 15 kbar to between 0.05 and 0.15 over a 175 °C temperature range (860–1035 °C, respectively). Using the same activities and conditions with a second equilibrium:

(4) 2 pargasite + 3 enstatite = 4 forsterite + 4 diopside + 2 jadeite + 3 Mg-Tschermak + 2 H_2O

Table 7. Compositions (weigh percent, measured by an electron probe microanalyzer) of apatite grains adjacent to the amphibole vein in peridotite.

	Ap-3	Ap-4	Ap-5	Ap-6	Ap-7	Ap-8	Ap-9	Ap-10
CaO	51.92	51.76	51.75	51.47	51.46	51.34	51.44	51.42
SrO	0.57	0.55	0.47	0.54	0.54	0.54	0.51	0.57
Na_2O	0.32	0.31	0.33	0.37	0.46	0.32	0.38	0.38
Ce_2O_3	0.003	0.057	0.326	0.154	0.20	b.d.	0.091	0.044
La_2O_3	0.07	0.035	0.019	0.100	0.06	0.018	0.143	0.027
FeO	0.39	0.37	0.51	0.42	0.45	0.44	0.47	0.48
P_2O_5	40.60	40.60	40.75	40.23	40.77	40.66	40.40	40.33
F	3.65	3.65	3.40	3.61	3.71	3.62	3.45	3.87
Cl	0.38	0.37	0.40	0.31	0.34	0.38	0.38	0.35
OH								
Atoms calculated per formula unit*								
Ca	9.758	9.739	9.700	9.62	9.663	9.68	9.717	9.728
Sr	0.052	0.056	0.048	0.054	0.055	0.055	0.052	0.058
Na	0.109	0.106	0.112	0.125	0.136	0.109	0.13	0.13
Ce	0.00	0.004	0.021	0.010	0.013		0.006	0.003
La	0.005	0.002	0.001	0.006	0.004	0.001	0.009	0.002
Fe	0.057	0.054	0.051	0.061	0.066	0.065	0.069	0.071
Sum	9.98	9.96	9.957	9.881	9.937	9.91	9.981	9.992
P	6.029	6.036	6.035	6.069	6.049	6.058	6.03	6.028
F	2.025	2.027	1.881	1.982	2.056	2.015	1.924	2.161
Cl	0.113	0.110	0.118	0.091	0.101	0.113	0.114	0.114
OH	−0.138	−0.137	0.001	−0.073	−0.157	−0.128	−0.037	−0.275

*Analyses recalculated using the program of Ketcham (2015) and a normalization based on an ideal structural formula of $X_{10}Y_6Z_2$.

Table 8. Pressure–temperature estimates for peridotite from two-pyroxene geothermometry (Brey and Köhler 1990) constrained by model geotherm (see Fig. 6).

Pair	*T* (°C)	Depth (km)	*P* (Gpa)
Matrix assemblage			
K101	991.2	49.31	1.43
K102	988.3	49.08	1.42
K103	1026.8	52.16	1.53
K104	1019.6	51.59	1.51
K105	1002.6	50.23	1.46
K106	1042.0	53.38	1.57
Average	1011.8	50.96	1.49
SD	21.256	1.702	0.060
Vein assemblage			
K-107	1038.3	53.09	1.56
K-108	1047.4	53.81	1.58
K-109	1002.6	50.23	1.46
K-110	1038.8	53.12	1.56
Average	1031.8	52.60	1.54
SD	19.890	1.590	0.054

yields very similar results (Fig. 7A) (a_{H2O} = 0.05–0.15 from 875 to 1040 °C).

If the fluid phase was poor in H_2O, the most likely additional component in the mantle would be CO_2. This was suggested by Lamb and Popp (2009) but they did not calculate the stability of their Ca-amphibole at elevated X_{CO2}, where we have to consider the stability of Ca–Mg carbonates. To do this calculation, we used the program TWEEQU (e.g, Berman 1991) with a mole fraction of CO_2 in the fluid of 0.9. The calculations outlined below show that for these *P*–*T* conditions, carbonate minerals would not be stable even with a fluid dominated by CO_2.

Using the same minerals as in equilibria 3 and 4 without the amphibole components, we can examine the reaction

(5) $\text{Diopside} + CO_2 = \text{Dolomite} + 2SiO_2$

At 1000 °C and 15 kbar, respectively, the equilibrium value of a_{SiO2} in eq. 4 is ≈0.5 and the activity of $CaMg(CO_3)_2$ is 1.0. These values can be substituted into eq. 5 with the activity of diopside = 0.60 and the activity of CO_2 = 0.9 to show the stability of these phases at the conditions of vein emplacement (Fig. 7B). These calculations and the absence of dolomite in these samples strongly suggest that pargasite and the associated peridotite minerals would be the stable phases at high values of a_{CO2} and low values of a_{H2O}.

Constraints from apatite

Apatite is present in the vein and in the matrix of the host lherzolite. O'Reilly and Griffin (2000) showed that the OH–F–Cl ratios in mantle apatite could be used to distinguish between different types of metasomatic fluids. They used textural arguments to suggest that higher F/Cl is consistent with a magmatic fluid. Although the textural features of an igneous origin, very coarse grain size (centimetre-sized crystals) and associated silicate minerals with igneous textures, were not observed in Craven Lake apatite, the dominance of F in the apatite from this sample is interpreted as evidence for a magmatic fluid phase. The small negative values for recalculated OH^- in the apatite (Table 7) are also consistent with the constraints from the composition and stability of the vein pargasite that demand a fluid with very low a_{H2O}.

Mineralogy and textures of the "veinlet"

A subordinate veinlet (~1 mm thick) extending from the amphibole vein described above was detected by a K-element X-ray map (Fig. 8). The veinlet does not consist of a single mineral but has a peridotitic mineralogy and complex textures suggesting a reaction relationship between minerals and a fluid phase (Fig. 9). For example, an embayment in one spinel grain is rimmed by an aggregate of fine-grained spinel crystals (Fig. 9A). The larger spinel crystal is compositionally similar to spinel crystals in the vein (Table 4, analyses 7–16), but the smaller spinels defining the rim are very rich in Cr (Table 4, analyses 17 and 18). Other minerals in the veinlet including clinopyroxene, olivine (high Mg), orthopyroxene (lower Mg large crystal), and pargasite have compositions similar to that found in the host peridotite (Table 9).

Olivine in reaction zones is variable in composition (Fig. 9A) and ranges from smaller crystals of Fo_{88} to larger crystals with core to

Fig. 6. Geothermometry results. (A) Estimates of equilibrium mantle temperatures from lherzolite sample based on two-pyroxene geothermometry (Brey and Köhler 1990); pairs of pyroxenes were analyzed within the host peridotite (black symbols) and within or adjacent to the amphibole vein (grey symbols). Dashed line indicates the average of each group. (B) Temperatures were calculated for pressures dictated by the *P*–*T* array of the model geotherm for the Cordillera (inset; after Greenfield et al. 2013). Geothermobarometry suggests that the sample derives from depths of 49–54 km (Table 6).

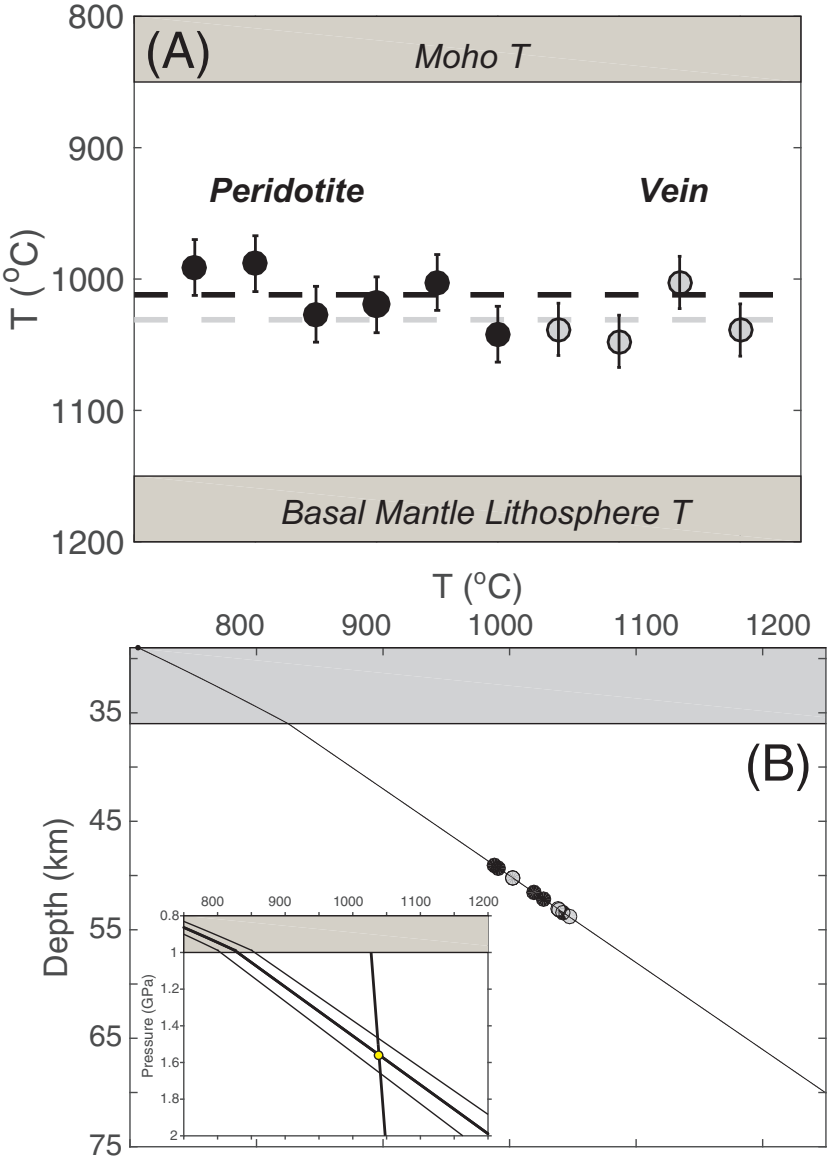

rim zoning of Fo_{83}–Fo_{88}. Olivine in the lherzolite host has an average composition of Fo_{75} with little zoning. A phase not observed elsewhere in the peridotite has been detected in two reaction areas (Fig. 9B). The phase locally is in contact with pargasite, suggesting a possible reaction. This phase is rich in Al and Si and contains significant K but has low Mg and Fe concentrations (Table 9). It is also notable for significant P_2O_5, which is not observed in other minerals. We cannot correlate this phase chemistry with any recognizable mineral stoichiometry. Although Martin (2007) described possible silicate melts that crystallized as a single mineral, this does not seem to be a likely possibility. We suggest that this is a glass from quenched melt that records either minor melting associated with the emplacement of the main vein or reaction between the vein fluid and the host lherzolite (Fig. 9).

Discussion

Within the northern North American Cordillera, only three occurrences of lithospheric mantle xenoliths have been previously reported to contain evidence for chemical modification or refertilization of the mantle lithosphere by H_2O-bearing fluids. Francis (1976) reported abundant interstitial amphibole in peridotite xenoliths from Quaternary volcanoes on Nunivak Island. This volcanism is part of the Bering Sea volcanic province and the xenoliths are samples of the mantle from the distal backarc setting of the Aleutian subduction zone. Brearley and Scarfe (1984) described interstitial amphibole in spinel lherzolite xenoliths from Lightening Peak (Fig. 1) situated in southeastern British Columbia, which also represents a distal backarc environment behind the Cascade arc. Canil and Scarfe (1989) reported interstitial phlogopite in dunites, lherzolites, and wehrlites at Kostal Lake (Fig. 1) within the Wells–Grey volcanic field in southeastern British Columbia. Canil and Scarfe (1989) observed that three is a strikingly low number considering the large number of known xenolith localities in British Columbia and the Yukon Territory (Fig. 1) (Edwards and Russell 2000).

Fig. 7. Mineral–fluid equilibria constraining the activities of volatile species. (A) T (°C)–a_{H2O} diagram calculated at 1.5 GPa for two different equilibria involving pargasite and anhydrous mantle minerals with a H_2O-bearing fluid (eqs. 3 and 4, see text). The two-pyroxene equilibration temperatures (990–1050 °C) imply low values of a_{H2O} (~0.12–0.16), suggesting low mole fractions of H_2O in the fluid/melt. (B) Temperature–a_{CO2} diagram at 15 kbar showing the equilibrium dolomite + SiO_2 = diopside + CO_2 and showing the stability limits of dolomite for these P–T–a_{CO2} conditions.

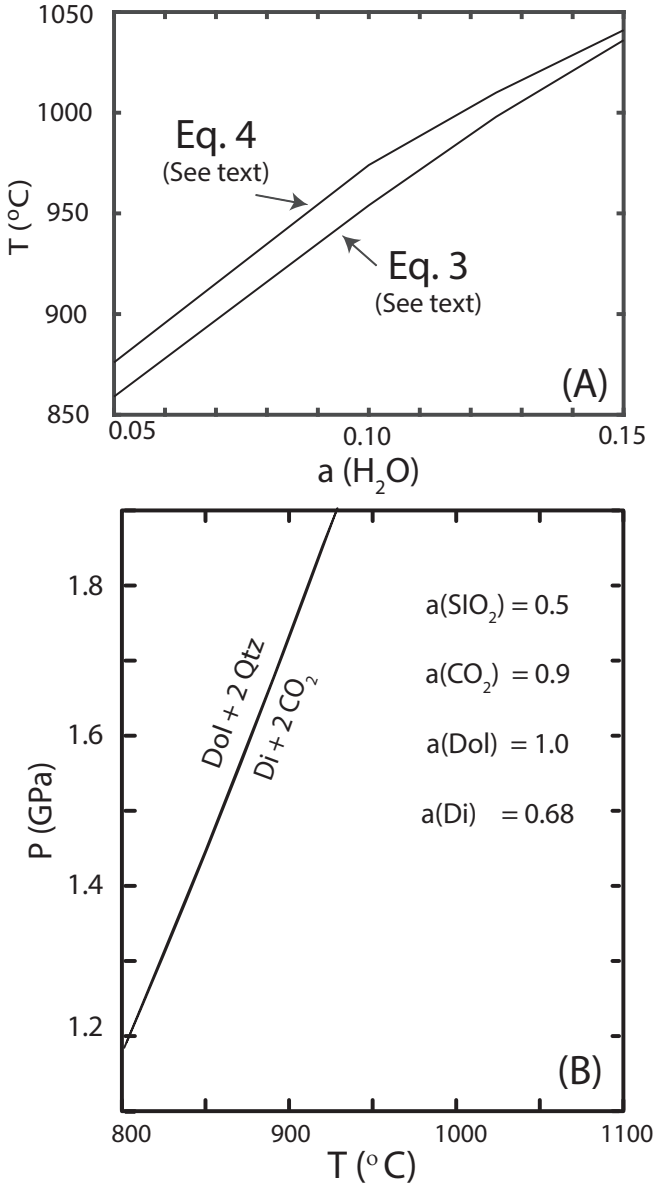

The Craven Lake occurrence is unique because the amphibole vein is in thermal but not textural equilibrium with the host mantle peridotite. The vein and vein minerals do not record the same deformation fabric (i.e., foliation) as the host lherzolite minerals, suggesting that the vein postdates the last lithospheric deformation event. The thermometry and geotherm model implies a source depth of 52 ± 2 km and a mantle temperature of ~1010–1030 °C. The presence of the vein indicates that an external fluid/melt created and filled a "fracture" at mantle depths.

Information from volatile-bearing minerals in the lithospheric mantle is critical for three reasons with respect to studies of the northern North American Cordillera lithosphere. Firstly, the minerals provide constraints on the impact of different tectonic processes on lithospheric formation. Secondly, the rheology of the mantle lithosphere can change significantly by the introduction of water (e.g., Dixon et al. 2004). Finally, the presence of volatile-rich phases can make the lithospheric mantle more susceptible to melting triggered by extensional stresses or increased asthenospheric heat flow (e.g., Francis and Ludden 1990; Shi et al. 1998).

Fig. 8. X-ray map showing K in the pargasite vein and the microveinlet branching off from the vein.

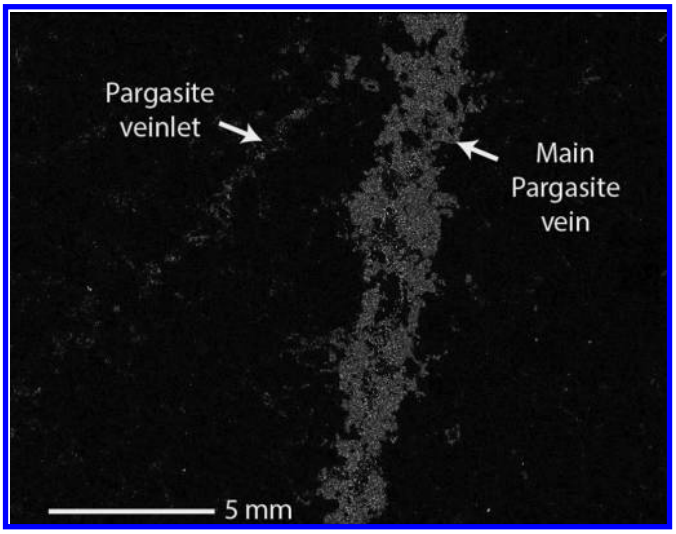

Timing of tectonic refertilization of the northern Cordilleran mantle lithosphere

The Canadian Cordillera has a complex history of terrane accretion and magmatism associated with subduction and with subsequent extension/transtension (cf. Polat et al. 2018 for a recent summary). Both of these processes could be accompanied by infiltration of fluids with distinct geochemical signatures into the mantle lithosphere. Given the broad span of time represented by the basement Stikine terrane (i.e., Late Paleozoic to Mid-Mesozoic) and the inferred Quaternary age of the Craven Lake volcanic deposits, the vein formation is likely tied to one of four petrotectonic events: (*i*) Triassic–Jurassic oceanic arc magmatism (e.g., Monger and Price 2002; Riddell 2011; many others), (*ii*) Late Jurassic – Early Cretaceous accretion and plutonism (e.g., Gibson et al. 2008; Riddell 2011), (*iii*) postaccretion subduction that lasted until the Eocene (e.g., Thorkelson and Taylor 1989; Haeussler et al. 2003), or (*iv*) Neogene to Recent transtension and alkaline magmatism (e.g., Edwards and Russell 2000; and many others).

Our work provides two critical observations that make the fourth event seem the most likely. Firstly, the pargasite vein is undeformed but clearly cuts the deformed matrix of the spinel lherzolite. The vein is cut off by the basanite host. The most obvious deformation event to have affected the Stikinia lithospheric mantle is Mesozoic accretion, so the vein probably postdates the first two petrotectonic events. Secondly, the mineral chemistry shows that the pargasite vein does not require the presence of an H_2O-dominated subduction zone fluid. Taken in conjunction with the presence of hydroxl-poor apatite, our analysis suggests that the vein is more likely to have formed in an environment having a greater affinity to the presence of alkaline silicate melts. This is consistent with the presence of mafic, transtensional NCVP magmatism spanning the Quaternary throughout the northern Stikine terrane and northwestern British Columbia. Manthei et al (2010) has given evidence for a broad-scale change in mantle geochemistry beneath the Coast Belt, immediately to the southwestern of Craven Lake, at about 10 Ma. If the pargasite vein is a record of this large-scale chemical change, its preservation shows that

Fig. 9. Electron backscatter images for microveinlet showing (A) an increase in Cr content of fine-grained spinel (~60 μm long) at the edges of the crystal (lighter grey), which is evidence for reaction localized at the edges of the crystal, and (B) breakdown reaction of a large pargasite crystal to olivine, clinopyroxene, and an unknown phase. Pargasite is about 200 μm long.

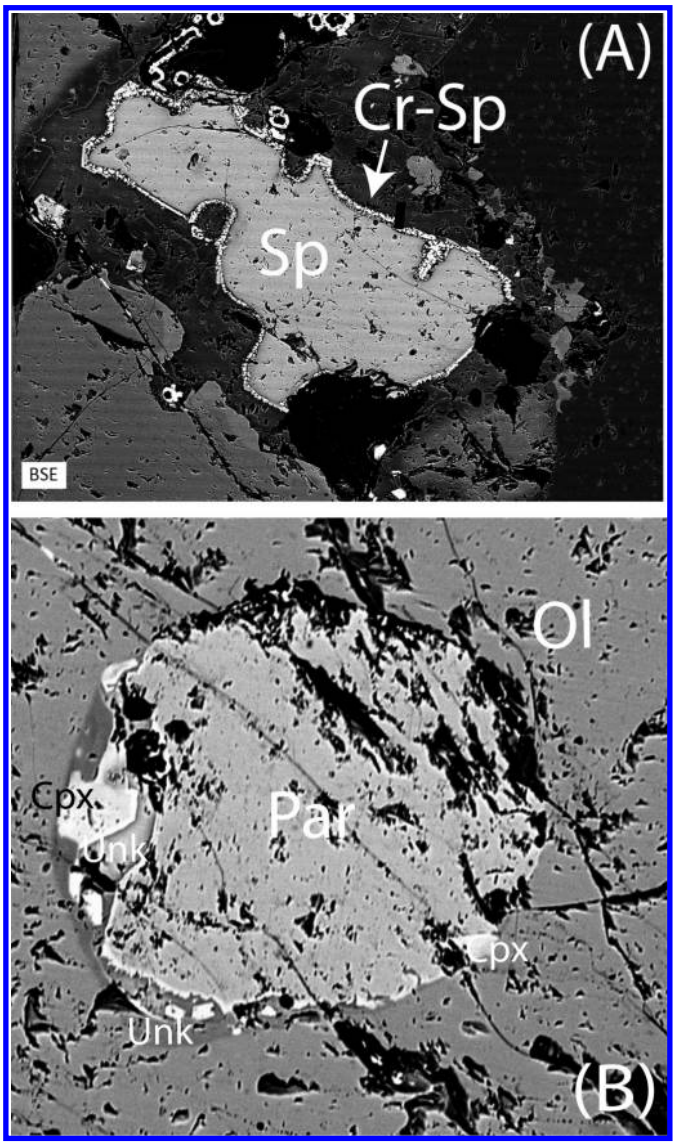

whatever the modification event (e.g., asthenospheric upwelling from a slab window or delamination from that or other causes), it did not totally remove the preexisting mantle lithosphere beneath Craven Lake.

"Weakening" of the Cordilleran Mantle lithosphere

Many recent studies have shown that lithospheric "hydration events" can change the rheology of anhydrous mantle minerals (e.g., olivine), which can lead to significant changes in the mechanical properties of the lithosphere and even "delamination events", where part of the mantle lithosphere detaches and founders downwards (Bao et al. 2014). While the vein formation is most likely associated with the Neogene to Recent magmatism of the NCVP, it is possible that it records events that facilitated delamination of older, subduction modified mantle lithosphere (e.g., Bao et al. 2014). Our work confirms that the vein-producing fluid was likely dominated by CO_2–F and not H_2O. However, our estimates for a_{H2O} of ~0.10–0.15 are sufficient to infuse mantle olivine with up to at least 50 ppm H_2O based on experimental studies (Padron-Navarta and Hermann 2017; Lamb and Popp 2009), which would have a significant impact for lowering the effective viscosity of the mantle lithosphere (Dixon et al. 2004). The presence of the pargasite vein and its cross-cutting relationship to the peridotite fabric might, both chemically (viscosity reduction) and physically (fabric discontinuities), weaken the mantle lithosphere and facilitate processes like delamination due to tectonic stress changes or to loading changes associated with repeated Quaternary ice loading and unloading. This in turn can produce substantial changes in the thickness of the lithosphere that drive isostatic uplift, changes in regional surface topography, and subsequent erosion and sediment transport (e.g., Hyndman and Lewis 1999; Bao et al. 2014).

Constraints on lithospheric melting in the northern Cordilleran

Several models have been presented to explain the diversity of primary magma compositions erupted in the Canadian Cordillera: (*i*) Nicholls et al. (1982) favoured derivation from the underlying "low velocity zone" (e.g., asthenospheric mantle), (*ii*) Francis and Ludden (1995) and Shi et al. (1998) favoured partial melting of the refertilized mantle lithosphere, and (*iii*) Edwards and Russell (1999, 2000) suggested partial melting at the base of the mantle lithosphere or upper asthenosphere. In particular, nephelinite within the British Columbia Cordillera has been ascribed to melting an amphibole-veined lithospheric mantle (e.g., Francis and Ludden 1995; Francis et al. 2010; Abraham et al. 2001, 2005; Polat et al. 2018).

Our model eq. 1 geotherm for the northern Cordillera and the *P*–*T* estimate for the pargasite-bearing xenolith narrowly constrain the potential source regions for xenoliths and lavas (Fig. 10). The host spinel lherzolite derives from the mantle lithosphere within the spinel stability field. The range of depth estimates (60–75 km) (Hammer and Clowes 2004) for the base of the seismically defined Lithosphere–Asthenospher Boundary (LAB) places the temperature of the LAB between 1100 and 1250 °C. If the base of the mantle lithosphere is taken to be 70 km, this corresponds to a temperature of 1200 °C, which is reasonable for hydrous liquidus temperatures for NCVP primary magmas (Edwards and Russell 2000). The source of the pargasite xenolith is within the pargasite stability field and approximately 50° below the dehydration breakdown curve. The xenolith is sourced from well below the anhydrous melting curve of peridotite but at temperatures above the H_2O-saturated peridotite melting curve. Hydrous lithosphere is likely more susceptible to melting events that can produce small volume eruptions like nephelinites. Clearly, even if the mantle lithosphere is hydrated, it must be strongly H_2O-undersaturated or the pargasite would have melted.

Given the model geotherm, pargasite is stable throughout the mantle lithosphere and into the LAB, supporting the Francis and Ludden (1995) model. However, the temperatures associated with basanite and nephelinite production are above the pargasite dehydration boundary. Thus, in this specific case (Craven Lake), production of the basanite magma by partial melting of an amphibole-bearing peridotitic source within the lithosphere is limited to the base of the lithosphere (~62–70 km) where the geotherm, basanite field, and pargasite dehydration fields intersect. This is also consistent with the fact that the basanite must source from depths greater than 52 ± 2 km to sample the pargasite-bearing xenolith. In the specific case of Craven Lake, a very narrow window exists for the formation of the host basanite magma by partial melting of the mantle lithosphere coinciding with the base of the mantle lithosphere (~62–70 km).

A second scenario allows for melting of the uppermost asthenosphere to produce the Craven Lake basanitic magma. The model geotherm and mantle adiabat imply temperatures at the base of the lithosphere and in the uppermost asthenosphere high enough

Table 9. Compositions (weight percent, compositions measured by an electron probe microanalyzer) and cation abundances of minerals and unknown phase from veinlet (see text) including standard deviation on five analyses of unknown phase.

	Par	Cpx12	Cpx-40	Unknown	SD	Cpx-K103
Oxide						
SiO_2	42.13	51.10	48.90	53.93	0.79	52.23
TiO_2	1.57	0.51	1.05	1.64	0.06	0.41
Al_2O_3	15.92	7.39	6.08	20.80	0.06	7.00
Cr_2O_3	0.72	0.72	1.81	0.04	0.03	
Fe_2O_3	3.76	4.17	4.98			1.24
FeO	3.45	0.20	0.24	4.73	0.45	3.79
MnO	0.08	0.08	0.11	0.08	0.02	0.14
MgO	15.98	15.81	17.33	3.07	0.06	14.7
CaO	10.34	19.83	20.30	8.49	0.75	19.36
Na_2O	3.44	1.67	0.60	2.53	0.33	1.70
K_2O	0.85			0.90	0.73	
Sum	98.24	101.48	101.40	99.88		100.57
Cation						
Si	6.00	1.82	1.76			1.88
Ti	0.17	0.01	0.03			0.01
Al	2.68	0.31	0.26			0.30
Cr	0.04	0.02	0.05			0
Fe^{3+}	0.40	0.11	0.14			0.03
Fe^{2+}	0.41	0.01	0.01			0.11
Mn	0.01	0.01	0.00			0.00
Mg	3.39	0.84	0.93			0.79
Ca	1.58	0.76	0.78			0.75
Na	0.85	0.12	0.04			0.12
K	0.16					
Sum	15.69	4.00	4.00			4.00

Note: Cations calculated from the AX program. Hornblende cations and ferric iron calculated on the basis of 23 oxygens. Clinopyroxene and ferric iron calculated on the basis of six oxygens.

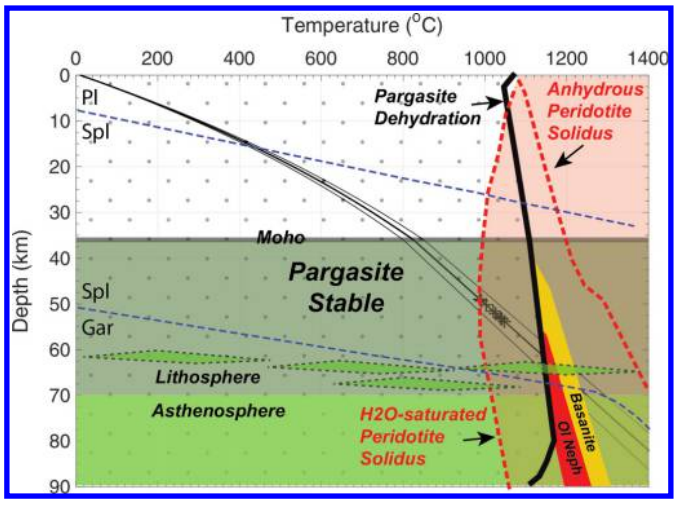

Fig. 10. Schematic cross section of the lithosphere underlying Craven Lake in the British Columbia Cordillera summarizing results of this study and the petrological and geophysical implications as a function of depth. The steady-state model geotherm for the crust and mantle lithosphere implies a MOHO temperature of ~850 °C and a source depth for the amphibole vein of ~52 ± 2 km. The *P*–*T* conditions are within the pargasite stability field (dotted pattern). The intersection of the geotherm at depth with the liquidus conditions for olivine nephelenite and basanite magmas suggests a lithosphere–asthenosphere boundary (LAB) at ~62 km within the spinel (versus garnet) stability field. The intersection of the model geotherm and the dehydration curve for pargasite (heavy black line) indicates that pargasite is not stable below the LAB.

to intersect the basanite melting field. The shallowest melting of the asthenosphere (>70 km) would be within the spinel stability field; melting at depths >70 km would be in the garnet stability field. Previous workers (e.g., Francis and Ludden 1990, 1995; Shi et al. 1998; Abraham et al. 2001) have argued that the trace element compositions of some NCVP lavas suggest melting of a garnet-bearing asthenospheric source. Their model for the origins of these magmas also requires amphibole in the source region (Francis and Ludden 1995), which is difficult to reconcile because at mantle depths >70 km, the temperatures are above the pargasite stability field.

We suggest that basanite and nephelenite magmas in the NCVP are produced by melting over a restricted depth at the base of the mantle lithosphere and the uppermost asthenosphere. This could explain some of the chemical diversity observed in NCVP lavas (Edwards and Russell 2000) in that more alkaline melts (i.e., nephelinites and basanites) may source from the mantle lithosphere, whereas alkali olivine basalts may have an asthenospheric source, as is traditionally proposed (e.g., Nicholls et al. 1982).

Conclusions

While mantle-derived peridotite xenoliths are relatively common globally in mafic alkaline volcanic deposits, it is much less common for those xenoliths to host volatile-rich phases as cross-cutting veins. This work documents the first known occurrence of such a vein from the northern part of the North American Cordillera, at Craven Lake British Columbia, and shows that the vein predominantly comprises pargasite amphibole and associated apatite, orthopyroxene, clinopyroxene, and spinel. A comparison to global occurrences of similar peridotite-hosted amphibole shows that pargasite, as opposed to kaersutite, is the most common type of amphibole in mantle peridotites. The presence of the coexisting phases in the Craven Lake vein constrains the chemical and physical conditions under which the vein presumably formed to be from a CO_2/F-dominated silicate melt emplaced at depths of

50 ± 2 km and temperatures of ~1050 °C. Based on previous studies, these conditions place the xenolith and vein within the relatively thin lithosphere of the Canadian Cordillera. Given that the vein cross-cuts a subtle deformation fabric in the host spinel lherzolite, whatever process formed the vein applied sufficient stress to fracture the lherzolite. A cryptic veinlet offshoot from the main vein highlights how grain boundary-controlled fluid migration produces different reaction textures that are indicative of reactive infiltration that likely produces more frequently documented interstitial pargasite at other xenolith localities.

While not overinterpreting the importance of one such xenolith, we tentatively conclude that the presence of even one pargasite-veined peridotite from the British Columbia lithospheric mantle has important implications for Cordilleran lithospheric processes and the generation of Neogene to Recent alkaline magmatism. Given the estimated stability limits of pargasite and the presence of F-rich apatite, the vein-forming phase was a CO_2-rich, H_2O-poor, relatively F-rich silicate fluid with trace element characteristics very similar to those exhibited by Quaternary mafic alkaline magmas (nephelinites and alkali olivine basalts) within the NCVP. Even though we have no direct constraints on the timing of vein formation, its chemical signature is most consistent with generation from small-degree partial melts from extensional lithospheric stresses as opposed to metasomatism associated with the subduction and accretion processes active during the Mesozoic to Eocene Cordilleran orogenies. The vein might be associated with Neogene to Recent, lithosphere-derived nephelinitic magmatism, either as an intrusive remnant or as source material. It is also possible that the introduction of volatile-rich silicate fluids like those responsible for the formation of the vein could facilitate recent lithospheric delamination within the northern Cordillera by forming fabric cross-cutting physical discontinuities or by reducing the viscosity of dominant mantle phases (i.e., olivine) by the addition of H_2O.

Acknowledgements

E.D.G. acknowledges financial support of his analytical work from an NSERC Discovery Grant. Thanks also to Rob Marr and Will Matthews for help with the electron microprobe and ICP-MS work. B.R.E. thanks C. Evenchick for first taking him to the Craven Lake site, K. Wetherell and M. Nogier for field assistance during the Craven Lake field work, and the Dickinson College Office of the Provost for financial support. Dickinson College students V. Tsang and C. Miller were instrumental in reconnaissance SEM studies of the Craven Lake xenolith suite and first identifying the amphibole vein. We thank D. Canil and an anonymous reviewer for comments that clarified and sharpened the text.

References

Abraham, A.C., Francis, D., and Polvé, M. 2001. Recent alkaline basalts as probes of the lithospheric mantle roots of the northern Canadian Cordillera. Chemical Geology, **175**: 361–386. doi:10.1016/S0009-2541(00)00330-2.

Abraham, A.C., Francis, D., and Polvé, M. 2005. Origin of recent alkaline lavas by lithospheric thinning beneath the northern Canadian Cordillera. Canadian Journal of Earth Sciences, **42**: 1073–1095. doi:10.1139/e04-092.

Bao, X., Eaton, D.W., and Guest, B. 2014. Plateau uplift in western Canada caused by lithospheric delamination along a craton edge. Nature Geoscience, **7**: 830–833. doi:10.1038/ngeo2270.

Berman, R.G. 1991. Thermobarometry using multi-equilibrium calculations: a new technique with petrologic applications. Canadian Mineralogist, **29**: 833–855.

Bénard, A., and Ionov, D.A. 2013. Melt- and fluid-rock interaction in suprasubduction lithospheric mantle: evidence from andesite-hosted veined peridotite xenoliths. Journal of Petrology, **54**: 2339–2378. doi:10.1093/petrology/egt050.

Boynton, W.V. 1984. Geochemistry of rare earth elements: meteorite studies. *In* Rare earth element geochemistry. *Edited by* P. Henderson. Elsevier, New York. pp. 63–114.

Brearley, M., and Scarfe, C. 1984. Amphibole in a spinel lherzolite xenolith: evidence for volatiles and partial melting in the upper mantle beneath southern British Columbia. Canadian Journal of Earth Sciences, **21**: 1067–1072. doi:10.1139/e84-111.

Brearley, M., Scarfe, C., and Fujii, T. 1984. The petrology of ultramafic xenoliths from Summit Lake, near Prince George, British Columbia. Contributions to Mineralogy and Petrology, **88**: 53–63. doi:10.1007/BF00371411.

Brey, G.P., and Köhler, T. 1990. Geothermobarometry in four-phase lherzolites II. New thermobarometers and practical assessment of existing thermobarometers. Journal of Petrology, **31**: 1353–1378. doi:10.1093/petrology/31.6.1353.

Canil, D., and Scarfe, C.M. 1989. Origin of phlogopite in mantle xenoliths from Kostal Lake, Wells Gray Park, British Columbia. Journal of Petrology, **30**: 1159–1179. doi:10.1093/petrology/30.5.1159.

Canil, D., Brearley, M., and Scarfe, C. 1987. Petrology of ultramafic xenoliths from Rayfield River, south-central British Columbia. Canadian Journal of Earth Sciences, **24**: 1679–1687. doi:10.1139/e87-161.

Canil, D., Virgo, D.M., and Scarfe, C. 1990. Oxidation state of mantle xenoliths from British Columbia, Canada. Contributions to Mineralogy and Petrology. **104**: 453–462. doi:10.1007/BF01575622.

Carignan, J., Ludden, J., and Francis, D. 1994, Isotopic characteristics of mantle sources for Quaternary continental alkaline magmas in the northern Canadian Cordillera. Earth and Planetary Science Letters, **128**: 271–286. doi:10.1016/0012-821X(94)90150-3.

Clowes, R.M., Zelt, C.A., Amor, J.R., and Ellis, R.M. 1995. Lithospheric structure in the southern Canadian Cordillera from a network of seismic refraction lines. Canadian Journal of Earth Sciences, **32**: 1485–1513. doi:10.1139/e95-122.

Clowes, R., Hammer, P., Fernandez-Viejo, G., and Welford, K. 2011. Lithospheric structure in northwestern Canada from Lithoprobe seismic refraction and related studies: a synthesis. Canadian Journal of Earth Sciences, **42**: 1277–1293. doi:10.1139/e04-069.

Colpron, M., and Nelson, J.L. 2011. A digital atlas of terranes for the Northern Cordillera [online]. Yukon Geological Survey. Available from www.geology.gov.yk.ca [accessed 2018].

Currie, C.A., and Hyndman, R.D. 2006. The thermal structure of subduction zone backarcs. Journal of Geophysical Research: Solid Earth, **111**. doi:10.1029/2005JB004024.

Dawson, J.B., and Smith, J.V. 1982. Upper-mantle amphiboles: a review. Mineralogical Magazine, **45**: 35–46. doi:10.1180/minmag.1982.045.337.04.

Dixon, J.E., Dixon, T.H., Bell, D.R., and Malservisi, R. 2004. Lateral variation in upper mantle viscosity: role of water. Earth and Planetary Science Letters, **222**: 451–467. doi:10.1016/j.epsl.2004.03.022.

Edwards, B.R., and Russell, J.K. 1999. Northern Cordilleran volcanic province: a northern basin and range? Geology, **27**: 243–246. doi:10.1130/0091-7613(1999)027<0243:NCVPAN>2.3.CO;2.

Edwards, B.R., and Russell, J.K. 2000. Distribution, nature and origin of Neogene-Quaternary magmatism in the northern Cordilleran volcanic province, Canada. Geological Society of America Bulletin, **112**: 1280–1295. doi:10.1130/0016-7606(2000)112<1280:DNAOON>2.0.CO;2.

Edwards, B.R., Russell, J.K., and Anderson, R.G. 2002. Subglacial, phonolitic volcanism at Hoodoo Mountain volcano, northern Canadian Cordillera. Bulletin of Volcanology, **64**: 254–272. doi:10.1007/s00445-002-0202-9.

Edwards, B.R., Evenchick, C.A., McNicoll, V., Nogier, M., and Wetherell, K. 2006. Overview of the volcanology of the Bell-Irving volcanic district, northwestern Bowser Basin, British Columbia: new examples of alpine glaciovolcanism from the northern Cordilleran volcanic province. Current Research, Geological Survey of Canada 2006-A3.

Fiesinger, D.W., and Nicholls, J. 1977. Petrography and petrology of Quaternary volcanic rocks, Quesnel Lake Region, east-central British Columbia. *In* Volcanic regimes in Canada. *Edited by* W.R.A. Baragar, L.C. Coleman, and J.M. Hall. Geologic Association of Canada Special Paper, **16**: 25–38.

Francis, A., and Ludden, D.J. 1990. The mantle source for olivine nephelinite, basanite, and alkaline olivine basalt at Fort Selkirk, Yukon, Canada. Journal of Petrology, **31**. doi:10.1093/petrology/31.2.371.

Francis, D.M. 1976. The origin of amphibole in lherzolite xenoliths from Nunivak Island, Alaska. Journal of Petrology, **17**: 357–378. doi:10.1093/petrology/17.3.357.

Francis, D.M. 1987. Mantle-melt interaction recorded in spinel lherzolite xenoliths from the Alligator Lake volcanic complex, Yukon, Canada. Journal of Petrology, **28**: 569–597. doi:10.1093/petrology/28.3.569.

Francis, D., and Ludden, J. 1995. The signature of amphibole in mafic alkaline lavas, a study in the northern Canadian Cordillera. Journal of Petrology, **36**: 1171–1191. doi:10.1093/petrology/36.5.1171.

Francis, D., Minarik, W., Proenza, Y., and Shi, L. 2010. An overview of the Canadian Cordilleran lithospheric mantle. Canadian Journal of Earth Sciences, **47**: 353–368. doi:10.1139/E09-072.

Frey, F.A., and Green, D.H. 1974. The mineralogy, geochemistry and origin of lherzolite inclusions in Victorian basanites. Geochimica et Cosmochimica Acta, **38**: 1023–1059. doi:10.1016/0016-7037(74)90003-9.

Friedman, E., Polat, A., Thorkelson, D., and Frei, R. 2016. Lithospheric mantle xenoliths sampled by melts from upwelling asthenosphere: the Quaternary Tasse alkaline basalts of southeastern British Columbia, Canada. Gondwana Research, **33**: 209–230. doi:10.1016/j.gr.2015.11.005.

Fujii, T., and Scarfe, C.M. 1982. Petrology of ultramafic nodules from West Kettle River, near Kelowna, Southern British Columbia. Contributions to Mineralogy and Petrology, **80**: 297–306. doi:10.1007/BF00378002.

Gabrielse, H., and Yorath, C.J. 1989. DNAG #4: The Cordilleran orogen in Canada. Geoscience Canada, **16**: 67–83.

Ghent, E., Edwards, B.R., Russell, J.K., and Mortensen, J. 2008. Granulite facies

xenoliths from Prindle volcano, Alaska: implications for the northern Cordilleran crustal lithosphere. Lithos, **115**: 344–358. doi:10.1016/j.lithos.2007.07.016.

Gibson, H.D., Brown, R.L., and Carr, S.D. 2008. Tectonic evolution of the Selkirk fan, southeastern Canadian Cordillera: a composite Middle Jurassic – Cretaceous orogenic structure. Tectonics, **27**: TC6007. doi:10.1029/2007TC002160.

Greenfield, A.M.R., Ghent, E.D., and Russell, J.K. 2013. Geothermobarometry of spinel lherzolites from southern British Columbia: implications for the thermal conditions in the upper mantle. Canadian Journal of Earth Sciences, **50**: 1019–1032. doi:10:1139/cjes-2013-0037.

Haeussler, P.J., Bradley, D.C., Wells, R.E., and Miller, M.L. 2003. Life and death of the Resurrection plate: evidence for its existence and subduction in the northeastern Pacific in Paleocene–Eocene time. GSA Bulletin, **115**: 867–880. doi:10.1130/0016-7606(2003)115<0867:LADOTR>2.0.CO;2.

Hammer, P.T.C., and Clowes, R.M. 2004. Accreted terranes of northwestern British Columbia, Canada: lithospheric velocity structure and tectonics. Journal of Geophysical Research, **109**(B06305): doi:10.1029/2003JB002749.

Hammer, P.T.C., Clowes, R.M., and Ellis, R.M. 2000. Crustal structure of N.W. British Columbia and S.E. Alaska from seismic wide-angle studies: Coast Plutonic Complex to Stikinia. Journal of Geophysical Research, **105**: 7961–7981. doi:10.1029/1999JB900378.

Hammer, P., Clowes, R.A., Cook, F., van der Velden, A., and Vasudevan, K. 2010. The Lithoprobe trans-continental lithospheric cross sections: imaging the internal structure of the North American continent. Canadian Journal of Earth Sciences, **47**: 821–857. doi:10.1139/E10-036.

Harder, M., and Russell, J.K. 2006. Thermal state of the upper mantle beneath the Northern Cordilleran Volcanic Province (NCVP), British Columbia, Canada. Lithos, **87**: 1–22. doi:10.1016/j.lithos.2005.05.002.

Hawthorne, F.C., Oberti, R., Harlow, G.E., Maresch, W.V., Martin, R.F., Schumacher, J.C. et al. 2012. Nomenclature of the amphibole group. American Mineralogist, **97**: 2031–2048. doi:10.2138/am.2012.4276.

Higgins, M.D., and Allen, J.M. 1985. A new locality of primary xenolith-bearing nephelinites in northwestern British Columbia. Canadian Journal of Earth Sciences, **22**: 1556–1559. doi:10.1139/e85-164.

Holland, T.J.B., and Blundy, J. 1994. Non-ideal interactions in calcic amphiboles and their bearing on amphibole–plagioclase thermometry. Contributions to Mineralogy and Petrology, **116**: 433–447.

Holland, T.J.B., and Powell, R. 1998. An internally consistent thermodynamic dataset for phases of petrological interest. Journal of Metamorphic Geology, **16**: 309–344. doi:10.1111/j.1525-1314.1998.00140.x.

Hyndman, R.D. 2010. The consequences of Canadian Cordillera thermal regime in recent tectonics and elevation: a review. Canadian Journal of Earth Science, **47**: 621–632. doi:10.1139/E10-016.

Hyndman, R.D. 2017. Lower-crustal flow and detachment in the North American Cordillera: a consequence of Cordillera-wide high temperatures. Geophysical Journal International, **209**: 1779–1799. doi:10.1093/gji/ggx138.

Hyndman, R.D., and Currie, C.A. 2011. Why is the North America Cordillera high? Hot backarcs, thermal isostasy, and mountain belts. Geology, **39**(8): 783–786.

Hyndman, R.D., and Lewis, T.J. 1999. Geophysical consequences of the Cordillera–Craton thermal transition in southwestern Canada. Tectonophysics, **306**: 397–422. doi:10.1016/S0040-1951(99)00068-2.

Ionov, D.A. 2010. Petrology of mantle wedge lithosphere: new data on suprasubduction zone peridotite xenoliths from the andesitic Avacha volcano, Kamchatka. Journal of Petrology, **51**: 327–361. doi:10.1093/petrology/egp090.

Ionov, D.A., O'Reilly, S.Y., Genshaft, Y.S., and Kopylova, M.G. 1996. Carbonate-bearing mantle xenoliths from Spitsbergen: phase relationships, mineral compositions and trace element residence. Contributions to Mineralogy and Petrology, **125**: 375–392. doi:10.1007/s004100050229.

Ionov, D.A., Griffin, W.L., and O'Reilly, S.Y. 1997. Volatile-bearing minerals and lithophile trace elements in the upper mantle. Chemical Geology, **141**: 153–184. doi:10.1016/S0009-2541(97)00061-2.

Jochum, K.P., Weis, U., Stoll, B., Kuzmin, D., Yang, Q, Raczek, I. et al. 2011. Determination of reference values for NIST SRM 610–617 glasses following ISO guidelines. Geostandards and Geoanalytical Research, **35**: 397–429. doi:10.1111/j.1751-908X.2011.00120.x.

Ketcham, R.A. 2015. Technical note: calculation of stoichiometry from EMP data for apatite and other phases with mixing on monovalent anion sites. American Mineralogist, **100**: 1620–1623. doi:10.2138/am-2015-5171.

Kukkonen, I.T., and Peltonen, P. 1999. Xenolith-controlled geotherm for the central Fennoscandian Shield: implications for lithosphere–asthenosphere relations. Tectonophysics, **304**: 301–315. doi:10.1016/S0040-1951(99)00031-1.

Lamb, W.M., and Popp, R.K. 2009. Amphibole equilibria in mantle rocks: determining values of mantle aH_2O and implications for mantle H_2O contents. American Mineralogist, **94**: 41–52. doi:10.2138/am.2009.2950.

Lewis, T.J., Bentkowski, W.H., and Hyndman, R.D. 1992. Crustal temperatures near the Lithoprobe southern Canadian Cordilleran transect. Canadian Journal of Earth Sciences, **29**: 1197–1214. doi:10.1139/e92-096.

Littlejohn, A.L., and Greenwood, H.J. 1974. Lherzolite nodules in basalts from British Columbia, Canada. Canadian Journal of Earth Sciences, **11**: 1288–1308. doi:10.1139/e74-121.

Manthei, C.D., Ducea, M.N., Girardi, J.D., Patchett, P.J., and Gahrels, G.E. 2010. Isotopic and geochemical evidence for a recent transition in mantle chemistry beneath the western Canadian Cordillera. Journal of Geophysical Research, **115**: B02204. doi:10.1029/2009JB006562.

Martin, R.F. 2007. Amphiboles in the igneous environment. *In* Amphiboles: crystal chemistry and human health. *Edited by* F.C. Hawthorne and R. Oberti. Reviews in Mineralogy and Geochemistry, **67**: 323–358. doi:10.2138/rmg.2007.67.9.

Miller, C., Edwards, B.R., Russell, J.K., and Peterson, N. 2010. Petrological imaging of the Cordilleran lithosphere beneath Craven Lake, NCVP, Canada: local evidence for a texturally diverse, hydrous lithosphere. EGU, Vienna, Austria, EGU2010-9245.

Moine, D.M., Cottin, J.-Y., Sheppard, S.M.F., Gregoire, M., O'Reilly, S.Y., and Giret, A. 2000. Incompatible trace element and isotopic (*D*/*H*) characteristics of amphibole- and phlogopite-bearing ultramafic to mafic xenoliths from Kerguelen Islands (TAAF, South Indian Ocean). European Journal of Mineralogy, **12**: 761–777. doi:10.1127/ejm/12/4/0761.

Monger, J., and Price, R. 2002. The Canadian Cordillera: geology and tectonic evolution. CSEG Recorder, February, 17–36.

Morales, L.F.G., and Tommasi, A. 2011. Composition, textures, seismic and thermal anisotropies of xenoliths from a thin and hot lithospheric mantle (Summit Lake, southern Canadian Cordillera). Tectonophysics, **507**: 1–15. doi:10.1016/j.tecto.2011.04.014.

Müller, W., Shelley, M., Miller, P., and Broude, S.S. 2009 Initial performance metrics of a new custom-designed ArF Excimer LA-ICPMS system coupled to a two-volume laser-ablation cell. Journal of Analytical Atomic Spectrometry, **24**: 209–214. doi:10.1039/B805995K.

Nicholls, J., Stout, M.Z., and Fiesinger, D.W. 1982. Petrologic variations in quaternary volcanic rocks, British Columbia, and the nature of the underlying upper mantle. Contributions to Mineralogy and Petrology, **79**: 201–218. doi:10.1007/BF01132888.

O'Reilly, S.Y., and Griffin, W.L. 2000. Apatite in the mantle: implications for metasomatic processes and high heat production in Phanerozoic mantle. Lithos, **53**: 217–232. doi:10.1016/S0024-4937(00)00026-8.

Padrón-Navarta, J.A., and Hermann, J. 2017. A subsolidus olivine water solubility equation for the Earth's upper mantle. Journal of Geophysical Research: Solid Earth, **122**: 9862–9880. doi:10.1002/2017JB014510.

Paton, C., Woodhead, J.D., Hellstrom, J.C., Hergt, J.M., Greig, A., and Maas, R. 2010. Improved laser ablation U–Pb zircon geochronology through robust downhole fractionation correction. Geochemistry Geophysics Geosystems, 11: Q0AA06.

Pearce, N.J.G., Perkins, W.T., Westgate, J.A., Gorton, M.P., Jackson, S.E., Neal, C.R. et al. 2007. A compilation of new and published major and trace element data for NIST SRM 610 and NIST SRM 612 glass reference materials. Geostandards Newsletter: The Journal of Geostandards and Geoanalysis, **21**: 115–144. doi:10.1111/j.1751-908X.1997.tb00538.x.

Peslier, A.H., Reisberg, L., Ludden, J., and Francis, D. 2000. Re–Os constraints on harzburgite and lherzolite formation in the lithospheric mantle: a study of Northern Canadian Cordillera xenoliths. Geochimica et Cosmochimica Acta, **64**: 3061–3071. doi:10.1016/S0016-7037(00)00391-4.

Peslier, A.H., Francis, D., and Ludden, J. 2002*a*. The lithospheric mantle beneath continental margins: melting and melt-rock reactions in Canadian Cordillera xenoliths. Journal of Petrology, **43**: 2013–2047. doi:10.1093/petrology/43.11.2013.

Peslier, A.H., Luhr, J.F., and Post, J. 2002*b*. Low water contents in pyroxenes from spinel-peridotites of the oxidized, sub-arc mantle wedge. Earth and Planetary Science Letters, **201**: 69–86. doi:10.1016/S0012-821X(02)00663-5.

Polat, A., Frei, R., Longstaffe, F.J., Thorkelson, D.J., and Friedman, E. 2018. Petrology and geochemistry of the Tasse mantle xenoliths of the Canadian Cordillera: a record of Archean to Quaternary mantle growth, metasomatism, removal, and melting. Tectonophysics, **737**: 1–26. doi:10.1016/j.tecto.2018.04.014.

Prescott, J. 1983, Petrogenesis of ultramafic xenoliths from the Canadian Cordillera and Alaska. Master's thesis, McGill University, Montreal, Quebec.

Riddell, J. 2011. Lithostratigraphic and tectonic framework of Jurassic and Cretaceous Intermontane sedimentary basins of south-central British Columbia. Canadian Journal of Earth Science, **48**: doi:10.1139/E11-034.

Ross, J.V. 1983. The nature and rheology of the Cordilleran upper mantle of British Columbia: inferences from peridotite xenoliths. Tectonophysics, **100**: 321–357. doi:10.1016/0040-1951(83)90193-2.

Sen, C., and Dunn, T. 1995. Experimental modal metasomatism of a spinel lherzolite and the production of amphibole-bearing peridotite. Contributions to Mineralogy and Petrology, **119**: 422–432. doi:10.1007/BF00286939.

Shi, L., Francis, D., Ludden, J., Frederiksen, A., and Bostock, M. 1998. Xenolith evidence for lithospheric melting above anomalously hot mantle under the northern Canadian Cordillera. Contributions to Mineralogy and Petrology, **131**: 39–53. doi:10.1007/s004100050377.

Sun, M., and Kerrich, R. 1995. Rare earth element and high field strength element characteristics of whole rocks and mineral separates of ultramafic nodules in Cenozoic volcanic vents of southeastern British Columbia, Canada. Geochimica et Cosmochimica Acta, **59**: 4863–4879. doi:10.1016/0016-7037(95)00341-X.

Thorkelson, D.J., and Taylor, R.P. 1989. Cordilleran slab windows. Geology, **17**: 833–836. doi:10.1130/0091-7613(1989)017<0833:CSW>2.3.CO;2.

Wilshire, H.C., Pike, J.E.N., Meyer, C.E., and Schwartzman, E.D. 1980. Amphibole-rich veins in lherzolite xenoliths, Dish Hill and Deadman Lake, California. American Journal of Science, **280A**: 576–593.

This article has been cited by:

1. J. Brendan Murphy. 2019. Appinite suites and their genetic relationship with coeval voluminous granitoid batholiths. *International Geology Review* **39**, 1-31. [Crossref]